Meteoritics & Planetary Science 44, Nr 10, 1561–1588 (2009)
Abstract available online at http://meteoritics.org

Kosmochloric Ca-rich pyroxenes and FeO-rich olivines (Kool grains) and associated phases in Stardust tracks and chondritic porous interplanetary dust particles: Possible precursors to FeO-rich type II chondrules in ordinary chondrites

D. J. JOSWIAK[1*], D. E. BROWNLEE[1], G. MATRAJT[1], A. J. WESTPHAL[2], and C. J. SNEAD[3]

[1]Department of Astronomy, University of Washington, Seattle, Washington 98195, USA
[2]Space Sciences Laboratory, University of California at Berkeley, Berkeley, California 94720, USA
[3]Department of Earth and Space Sciences, University of California, Los Angeles, California 90095, USA
[*]Corresponding author. E-mail: joswiak@astro.washington.edu

(Received 19 May 2009; revision accepted 22 October 2009)

Abstract–Terminal particles and mineral fragments from comet 81P/Wild 2 were studied in 16 aerogel tracks by transmission and secondary electron microscopy. In eight tracks clinopyroxenes with correlated Na_2O and Cr_2O_3 contents as high as 6.0 wt% and 13.0 wt%, respectively, were found. Kosmochloric (Ko) clinopyroxenes were also observed in 4 chondritic interplanetary dust particles (IDPs). The Ko-clinopyroxenes were often associated with FeO-rich olivine ± Cr-rich spinel ± aluminosilicate glass or albitic feldspar, assemblages referred to as Kool grains (Ko = kosmochloric Ca-rich pyroxene, ol = olivine). Fine-grained (submicron) Kool fragments have textures suggestive of crystallization from melts while coarse-grained (>1 μm) Kool fragments are often glass-free and may have formed by thermal metamorphism in the nebula. Average major and minor element distributions between clinopyroxenes and coexisting FeO-rich olivines are consistent with these phases forming at or near equilibrium. In glass-bearing fine-grained Kool fragments, high concentrations of Na in the clinopyroxenes are inconsistent with existing experimentally determined partition coefficients at equilibrium. We speculate that the availability of Cr in the melt increased the clinopyroxene Na partition coefficient via a coupled substitution thereby enhancing this phase with the kosmochlor component. The high temperature minerals, fine-grain sizes, bulk compositions and common occurrence in the SD tracks and IDPs support the idea that Kool grains could have been precursors to type II chondrules in ordinary chondrites. These grains, however, have not been observed in these meteorites suggesting that they were destroyed during chondrule formation and recycling or were not present in the nebula at the time and location where meteoritic chondrules formed.

INTRODUCTION

The return of samples by the Stardust (SD) spacecraft in January 2006 from comet 81P/Wild 2 has provided a wealth of information on materials that accreted to form objects that make up the Kuiper belt. Jupiter family comets such as Wild 2 that formed in the Kuiper belt are thought to represent primitive bodies that accreted in the solar nebula ~4.6 Ga and as such are expected to contain solids that were the primordial building blocks of the solar system (Brownlee et al. 2006). To date, researchers have reported a large range of materials including Fe-Mg silicates, oxides, Fe+Ni sulfide minerals, silicate glass, carbonaceous phases, calcium aluminum inclusions (CAIs), chondrule-like grains, presolar SiC and other unidentified presolar materials (Zolensky et al. 2006; Joswiak et al. 2007; Simon et al. 2008; Nakamura et al. 2008; Matrajt et al. 2008; Messenger et al. 2009) in the SD tracks. Most of the minerals formed at relatively high temperatures, above ~1000 °C, providing an early view that indicates much of the matter that composes comet Wild 2 formed in the hot inner region of the nebula (Nakamura et al. 2008; Simon et al. 2008). The high temperature materials that formed in the inner nebula were apparently transported outward to the Kuiper belt region (Shu et al. 1997; Ciesla and Cuzzi 2007) where they combined with ices to form comets.

Using TEM as a principle means of investigation, we have examined terminal particles and large mineral fragments extracted from 16 tracks and were surprised to find a high abundance of Ca-rich pyroxenes containing a significant kosmochlor component (enriched Na and Cr). The clinopyroxenes are often associated with FeO-rich olivines, Cr-rich spinel (chromite) and Al-rich silicate glass or albitic

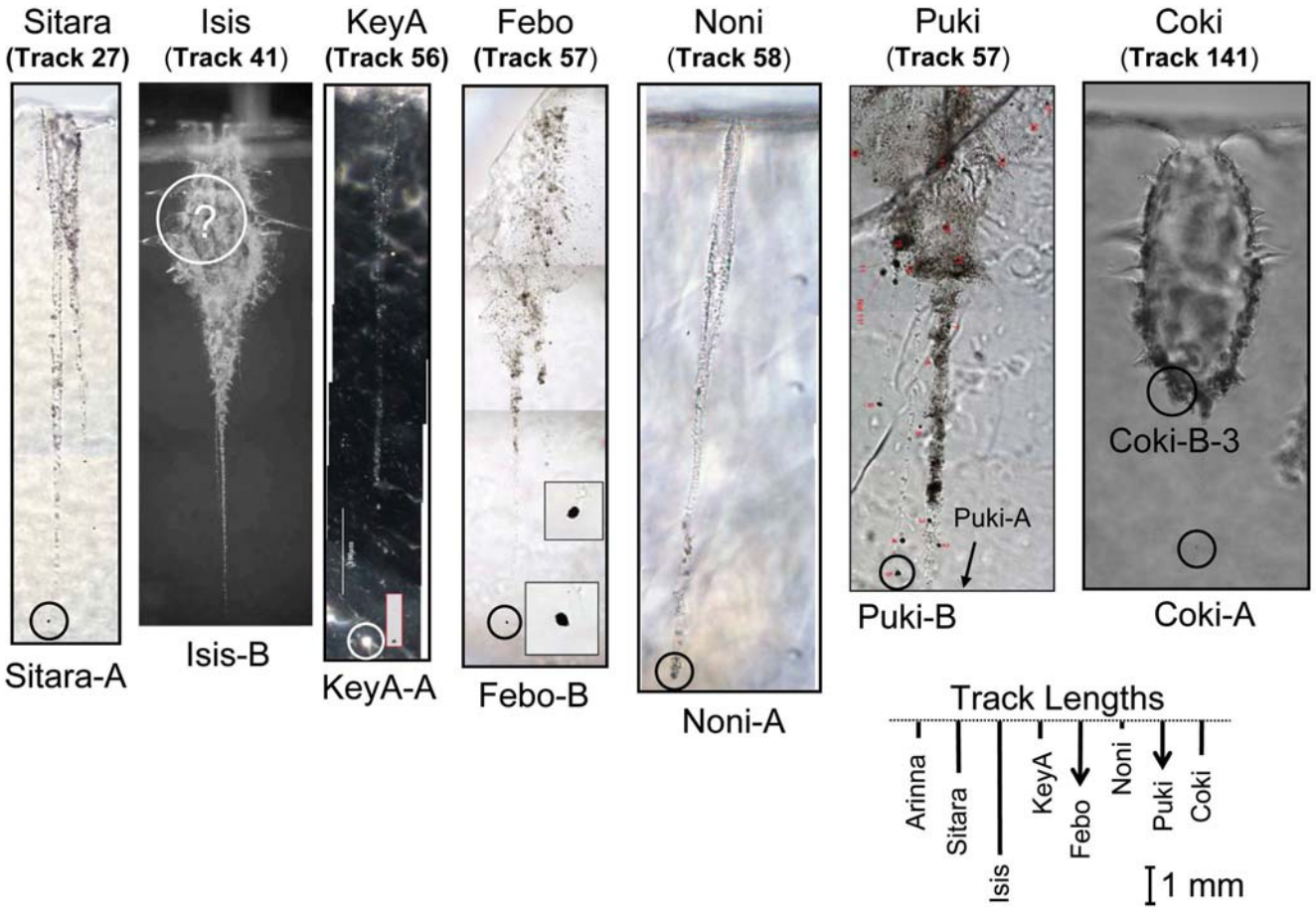

Fig. 1. Optical images of the cross sections of 7 of the 8 SD tracks discussed in this study. University of Washington track names and NASA/JSC track numbers are given above each track image and correlate to track names and numbers listed in Table 1. Specific University of Washington names of terminal particles and wall fragments that were removed from the tracks and microtomed are given beneath each image. Their locations in the tracks are shown by the solid circles. Track 57 TP (Puki-A) location is below the bottom of the image. Absolute track lengths from all 8 tracks are shown in the bottom right-hand side of the figure. Note 1 mm scale bar. Arrows on tracks Febo and Noni indicate that these are minimum lengths for these tracks. The circled area with question mark in Isis indicates probable area of fragment location.

feldspar and clearly formed at high temperatures. Some of the kosmochloric clinopyroxene assemblages display igneous textures on a submicron scale suggesting crystallization from silicate melts, while others have textures that can be interpreted as either igneous or metamorphic. Surprisingly, we have also observed similar assemblages in chondritic porous interplanetary dust particles (CP IDPs), some of which may have their origins in comets (Brownlee et al. 1993, 1994; Joswiak et al. 2005) indicating that these assemblages occur in primitive fine-grained cosmic dust.

In this paper, we present detailed mineralogic results of the kosmochloric clinopyroxene assemblages and attempt to interpret their origins. We focus on the Ko-clinopyroxene + FeO-rich olivine ± chromite ± Al-silicate glass assemblages and use the term "Kool" fragment or "Kool" grain (Ko-clinopyroxene + FeO-rich olivine) to refer to this assemblage. Given their submicron to micron grain sizes, formation at high temperatures and unusually high abundance in the SD tracks and occurrence in CP IDPs, we discuss whether Kool fragments may be previously unrecognized early solar nebula products and thus possible precursors to some types of chondrules.

SAMPLE PREPARATION AND ANALYTICAL TECHNIQUES

We found Ko-bearing clinopyroxenes in 8 of 16 aerogel tracks (Fig. 1). The comet dust grains were present as terminal particles (TP) and as fragments entrained along track walls. As each track was unique in shape and size and number of particles present, special care was taken to optically examine each track prior to sample preparation. The samples were prepared by keystoning individual tracks from aerogel blocks at the University of California, Berkeley (Westphal et al. 2004) followed by flattening between pre-cleaned glass slides and embedding with acrylic (Matrajt and Brownlee 2006). Stairstep mesas were cut around the fragments in each mount with the top square trimmed to approximately 100 μm on

each side followed by microtoming with a 45-degree diamond knife on a Leica Ultracut S ultramicrotome. The resultant microtome sections, typically 70–100 nm thick, were removed from a water-filled boat and placed onto C-thin films attached to 200-mesh Cu or Au TEM grids.

The interplanetary dust particles were obtained through the curation facility at the Johnson Space Center and embedded in epoxy resin and microtomed in a similar way as the SD particles. Prior to ultramicrotomy the bulk compositions of two of the four IDPs (U2073A-9A and U2073B-4F) were measured by scanning electron microscopy under a previous study (Love et al. 1994).

All microtome sections were studied with a 200 kV Tecnai F20 field-emission STEM, equipped with bright-field/dark-field CCD cameras and high angle annular dark-field (HAADF) and secondary electron STEM detectors. EDX analyses were carried out with a low background beryllium holder with double-tilt capability. TEM EDX data were collected and quantified with an EDAX X-ray detector with light element capability and a stand-alone EDAX Genesis EDX system operating in parallel to the embedded Tecnai EDX system. In nearly all cases, EDX spectra were collected by broad beam analysis in conventional TEM mode by condensing the electron beam (typically 50–100 nm in diameter) to the region of interest. This method was used instead of STEM mode to minimize beam damage to the samples. Difficulties, however, arose with determining the compositions of many of the glasses due to the problems of element volatilization during analysis. Good compositional analyses were difficult to obtain on poorly crystalline Na-Al silicates even under low dose conditions. EDX peak integrals were determined using the Genesis fitting routines after background subtraction. EDX detector energy calibration was done with a Cu and Al thin-film prepared at the University of Washington. K-factors were measured for all elements using a NIST SRM 2063a thin-film standard and well-characterized mineral standards which were previously crushed or microtomed and placed onto TEM grids. Where possible, multiple mineral standards were used for measurement of k-factors. Relative errors are better than 5% for major elements and 15–20% for minor elements. Measurements of the V contents in the spinels are likely to have greater uncertainties due overlapping $V_{K\alpha}$ and $Ti_{K\beta}$ spectral peaks.

High-resolution lattice fringe imaging and electron micro-diffraction were used to measure atomic planar spacings of individual minerals. The measured d-spacings between diffraction spots and their associated angles were compared to XRD data on published minerals from the Mineral Powder File Data Book (Bayliss et al. 1980) to make mineralogical identifications. Well-known mineral standards were used for calibration for both high-resolution TEM images and electron diffraction (ED) patterns. Estimated errors, based on examination of minerals and other standards indicate that measurement errors were typically less than about 5% for both HRTEM and ED patterns. Angular measurements between reflections in the diffraction patterns have errors of less than 2 degrees.

Ideally, it was desirable to study both the microtome sections and the corresponding potted butts of the SD particles. Grain relationships between phases are often obscured in microtome sections which contain redistributed shards from the microtoming process. Observing embedded grains in potted butts that are within a few microtome sections of a studied TEM grid provided a much clearer picture of the phase relationships as minerals and glass generally remain intact in the potted butts. Thus, to compliment the TEM studies we observed the Wild 2 samples with backscatter electrons in a FESEM, when possible. The FESEM used in this study was a JEOL JSM 7000F equipped with an EDAX X-ray analyzer with light element capability and SE and backscatter detectors. With the FESEM, BSE images were typically collected at 10 KV using minimal beam currents due to the high susceptibility to shrinkage of the acrylic resin in the electron beam.

STARDUST TRACKS

Track Nomenclature

The distribution of Wild 2 fragments within the SD tracks and the textural and compositional ranges of minerals present within a single track is typically complex, and thus reference to the various particles can be confusing, so we briefly define terms and names of particles that were studied throughout this paper. We use the term “particles” (in the generic sense) to refer to solids that were derived directly from Wild 2 prior to their encounter with the Stardust spacecraft. Most particles impacting aerogel were disaggregated into smaller pieces called “fragments” and were lodged along track walls or came to rest at the end of a track to become a terminal particle (TP). In some cases fragments are visible at the termini of shorter tracks that are subparallel to the main track; we refer to these as fragments and not terminal particles.

Sample numbers were given to each track during the preliminary examination stage at the NASA-JSC curatorial facility. We chose to give unique names to each track, typically from Egyptian gods or goddesses. The University of Washington track names and their corresponding track numbers are listed in Table 1, columns 1 and 2, respectively. The listed track numbers given in the table are the same as those listed on the NASA Stardust catalog web page: curator.jsc.nasa.gov/stardust/sample_catalog/index.cfm.

Because most tracks contain one or more large minerals or mineral assemblages which are present as terminal particles (TP) or fragments lodged along walls or at the termini of short subtracks, these fragments are named based on parent track name followed by a letter or letter and number combination. For instance, track 141 was given the name Coki while two fragments that were studied in the track, one a TP and the other a fragment lodged along the track wall and

Table 1. Names, mineralogy, textures and grain sizes in Wild 2 fragments and IDPs that contain Ko-bearing clinopyroxenes.

UW track name or IDP	JSC track #/ IDP #	Fragment name	Fragment type	Track type[1]	Projectile diameter (μm)[1]	Texture	Grain size (μm)	Fragment mineralogy	Other minerals in track or IDP
				Wild 2 fragments—Fine-grained					
Arinna	10	Arinna-A-1	Wall?	B?	3	xtls+gl	0.1–0. 2	Ko-aug, $Fo_{88–93}$, alb?, chr, gl, pyrr	Fo_{98}, pyrr
Febo	57	Febo-B	TP	B	>9	xtls+gl	0.1–0.2	Ko-diop, gl, pent, pyrr, Fo_{97},En_{98}	Fo_{97}, En_{98}
Noni	58	Noni-A	TP	A	1.5	xtls+gl	0.1–0.2	Ko-aug, $Fo_{90–95}$, gl, FeNi oxide	None observed
Coki	141	Coki-A	TP	B	8	xtls+gl	0.1–0.2	Ko-aug, $Fo_{80–88}$, gl	CAI?, En
				Wild 2 fragments—Coarse-grained					
Sitara	27	Sitara-A	TP	A	6	xtls	≥1	Ko-aug, $En_{80–86}$, pent, pyrr	
Isis	41	Isis-B	Wall	B	35	xtls	≥1	Ko-aug, $Fo_{69–72}$	En, trid
KeyA	56	KeyA-A	TP	A	3	xtls	≥1	Ko-aug, En, roed, chr, gl[2]	More work needed
Puki	77	Puki-A	TP	B	>6	xtls	≥1	Ko-aug, $Fo_{69–72}$	Fo_{99}, pent, FeNi mtl, schr, sp
Puki	77	Puki-B	Wall	B	>6	xtls	≥1	Ko-aug/ diop, $Fo_{65–69}$,alb?	Fo_{99}, pent, FeNi mtl, schr, sp
Coki	141	Coki-B-3	Wall	B	8	xtls	≥1	Ko-aug, $Fo_{84–85}$,alb?, chr	CAI?, En
				Interplanetary dust particles—Fine-grained					
U2073A-9A	IDP2	–	–	–	–	xtls+gl?	0.1–0.5	Ko-aug, $Fo_{76–82}$,alb?, an, chr, gl, pent	pyrr, pent, breun, wo,
U2073B-4F	IDP3	–	–	–	–	xtls	≥0.5	Ko-aug, $Fo_{69–75}$, pyrr, FeNi mtl	pyrr
U2-20: SP75	IDP4	–	–	–	–	xtls+gl	0.1–0.5	Ko-aug, $Fo_{77–83}$, alb, pyrr, gl	En. Mt, Na-merr?
				Interplanetary dust particle—Coarse-grained					
U2-20A14	IDP1	–	–	–	–	xtls+gl	≥1	Ko-aug, $Fo_{63–65}$, chr, gl	Fe-sulfide

[1]Track type and projectile diameter estimates after Burchell et al. (2008). [2]Glass believed to be a result of amorphization during collection. Coki-A and Coki-B are separate fragments extracted from track 141. Puki-A and Puki-B are separate fragments extracted from track 77. Key: UW = University of Washington, JSC = (NASA) Johnson Space Center, IDP = interplanetary dust particle, xtls = crystals, gl = glass, Ko-aug = kosmochloric augite, Ko-diop = kosmochloric diopside, Fo = forsterite, alb = albite, an = anorthite, chr = Cr-rich spinel, gl = silicate glass, pyrr = pyrrhotite, pent = pentlandite, En = enstatite trid = tridymite, roed = roedderite, FeNi mtl = Fe + Ni metal alloy, schr = schreibersite, CAI = calcium aluminum inclusion, breun = breunnerite carbonate, wo-wollastonite, Mt = magnetite, merr = merrillite.

near the bottom of the large bulbous cavity are labelled Coki-A and Coki-B-3, respectively (Fig. 1; Table 1, column 3). Fragments are typically one micron or more in size and may be composed of either a single phase or multiple phases; the term assemblage is used to denote a TP or fragment in a track composed of more than a single phase and could be thought of as a "nanorock."

Track Morphology

We have examined portions of 8 tracks which variously contain large fragments composed of single mineral grains or mineral assemblages and fine-grained melted material. The eight tracks are listed in Table 1, which gives textures, typical mineral grain sizes, track locations of the fragments, and

other minerals observed in the tracks. Seven cross-sectional profiles of the tracks are shown in the optical images in Fig. 1. Due to erosional abrasion and particle disaggregation that occurred during deceleration in aerogel most of the tracks are petrographically complex being composed of disseminated fragments and melt which were dispersed to numerous locations along the track lengths. Though this has complicated interpretations as to what cogenetic relationships, if any, existed between the different fragments within individual tracks, it is often clear, based on mineral compositions and relative locations, that some fragments were physically connected prior to impact.

Burchell et al. (2008) classified Stardust tracks into three categories depending on the shapes of their cross-sectional profiles. Carrot-shaped tracks are typified by monotonically decreasing widths from the top of the track to the terminal particle. These tracks, classified as type A, are typically thin and were formed by a competent particle that did not disaggregate during collection. At least three tracks—Sitara, Key A and Noni—are believed to be type A (Fig. 1 and Table 1). Tracks which have a wide bulbous region near their entry points and then taper down toward their terminal particles are classified as type B. These tracks often contain complex mineral assemblages mixed with aerogel melt because the impacting particles were composed of less competent materials that were easily broken into smaller fragments during collection. It is likely that the primary incident particles in type B tracks were composites of small and large minerals or mineral aggregates and fine-grained matrix material. Obviously, type B tracks provide more of a challenge to interpret petrographically as it is often unclear what associations, if any, existed between the various fragments within these tracks. At least four tracks—Isis, Febo, Puki, and Coki,—appear to be type B tracks (Fig. 1 and Table 1). No optical images exist for Arinna, the eighth track in this study. It was flattened axially and believed to have been a type B track.

Could Kool Fragments Have Formed from Impact Heating Into Aerogel?

Assemblages of kosmochloric Ca-rich pyroxene, FeO-rich olivine +/− Cr-rich spinel +/− aluminosilicate glass have been found in roughly half of the aerogel tracks that we have examined from Stardust. An important question is whether any or all of the components may have formed during high-speed capture in silica aerogel. While it is presently not possible to assertively rule this out, we see no evidence for capture-induced production of any phases inside micron and larger solid particles captured by Stardust. It therefore seems unlikely that the unusual mix of materials in Kool grains would form by capture heating. The finding of Kool assemblages in unmelted IDPs appears to be proof that these materials exist in primitive Solar System materials and are not odd products related to capture heating. In somewhat analogous pulse-heated meteoritic materials including partially melted micrometeorites and fusion crusts of primitive meteorites, even after years of analyses, we have never noted anything similar to Kool grains.

For captured Stardust particles, the common survival of irregular unmelted sulfide grains as micron and larger particles is evidence the interiors of micron and larger grains were not heated above ~1000 °C during capture. Strong alteration did occur on Stardust materials but this seems to have been confined to submicron surface layers of larger than micron particles and submicron material that sloughed off particles during deceleration in aerogel. In the upper parts of tracks, when particles are still traveling >3 km/s, they are surrounded by a thin sheet of melted silica which must have a temperature near 2000 °C. Evidence for this process is seen as silica melt lining the upper parts of track walls as well as vesicular silica melt that is sometimes attached to captured particles. The heating effects during capture occur on very short time scales. At the initial entry speed, when the thermal power generation is highest, a 5 μm particle travels its own diameter in a nanosecond. Due to the nanosecond to microsecond time scale of the projectile-aerogel interactions, thermal damage to micron and larger solid particles is limited to a very thin skin depth. When projectile material does melt it is abraded off and carried away by the surrounding flow of silica. In essentially all cases of greater than micron particles, microtome sections show that the boundary between projectile and aerogel melt is sharp indicating temperature gradients on the order of a thousand degrees per micron. Somewhat analogous to laser ablation, the affected material is removed but due to the high temperature gradient, the underlying material is well preserved.

The issue of glass in comet particles is an important one. Except for very rare cases, we see no evidence of intrusion of molten silica into particles. Pulse heating can produce glass and the captured projectiles are surrounded by molten silica during deceleration. When aerogel melt is seen near projectile edges it is often nearly pure silica. In cases where projectile materials and aerogel melt have mixed, the projectile component is often minor, consistent with significant dilution. We know of no way to prove that the glass in Kool grains is cometary but we have no evidence that glass of this composition is significantly produced during capture. The glass compositions for chondrule fragments captured from Comet Wild 2 have compositions consistent with the range of mesostasis glass compositions of meteoritic chondrules; in particular their internal differences of oxygen isotopic compositions are not consistent with significant modification during capture in aerogel (Nakamura et al. 2008).

RESULTS

Fine-Grained Fragments

In SD tracks Arinna, Febo, Noni and Coki, Ko-calcic

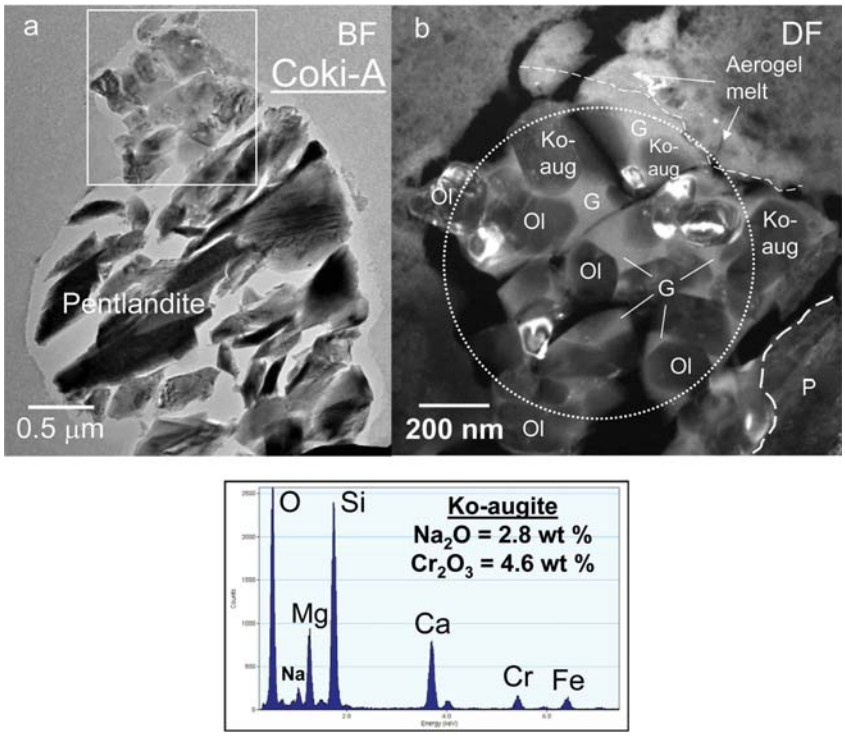

Fig. 2. a) Bright-field image of terminal particle from track 141 (Coki) showing large pentlandite grain with attached Kool grain. b) Dark-field image of outlined square in (a) showing detail of kosmochloric augites, FeO-bearing olivines and Mg-Al-Fe-bearing silicate glass (Kool grain). Heavy dashed white line shows edge of attached pentlandite. Lighter dashed white line near the top of the figure gives approximate contact between Kool grain and aerogel melt. Dotted circle shows region where bulk composition was obtained (See text). It is likely that this fragment is a small remnant of a much larger Kool grain that disaggregated during capture in aerogel. Ol = olivine, Ko-aug = kosmochloric augite, G = glass, P = pentlandite.

pyroxenes occur in fine-grained assemblages with FeO-bearing olivine +/− chromite +/− aluminosilicate glass. The morphologies of Coki-A and Arinna-A-1 resemble porphyritic textures typical of terrestrial volcanic rocks suggesting growth of phenocrysts from a melt (Figs. 2b and 3a). Examination of microtome slices of fragment Coki-A (Fig. 2b) shows an assemblage composed of Ko-augite and FeO-rich olivine crystals 100–200 nm in size with interstitial aluminosilicate glass. We observed this assemblage attached to a large pentlandite TP (Fig. 2a) along a sharp contact. The original size of the impacting object which contained this assemblage was apparently much larger than appears in the figure as portions of it were torn off during capture into aerogel. We have observed numerous fragments with similar mineralogy and texture in the same track which we infer were part of a larger coherent particle which fragmented during capture. The rounded exterior of the larger pentlandite grain suggests abrasion along its edges during capture.

Figure 3a from Track 10 (Arinna) shows a 0.6 μm wide region composed of olivine crystals, Ko-augite and glass similar to Coki-A (Fig. 2b). In the figure, 200 nm and smaller subhedral crystals of Fo_{93} and Ko-augite are present with interstitial regions of Al-bearing silicate glass. This fragment was isolated from other similar fragments in the track and was discussed by Zolensky et al. (2006). Ko-augite and FeO-bearing olivines of similar compositions were observed attached to a >2 μm pyrrhotite grain (Figs. 3b and 3c), indicating that this isolated fragment was originally part of the Kool assemblage shown in Fig. 3b which separated during capture. A ~300 nm pyrrhotite crystal that is present along the edge of the Kool assemblage in Arinna-A-1 (Fig. 3a) has a similar composition to the larger TP shown in Fig. 3b suggesting its former attachment to the Fe-sulfide TP.

The TP in Track 57 (Febo) is composed of a large pyrrhotite grain with apparent size of 2 μm and an equal volume of attached fine-grained crystalline silicates, silicate glass, Ni-rich Fe-sulfides and minor carbonaceous material (Fig. 4). Isotopic analyses of the carbonaceous material have shown it to have ^{15}N enrichments (Matrajt et al. 2008). Embedded within this region of fine-grained material we observed a 200 nm Ko-diopside crystal with well-faceted crystal faces in contact with Al-silicate glass (Fig. 4b). Surrounding this feature are <200 nm Ni-rich Fe-sulfides decorating the perimeter of the Ko-diopside/glass assemblage. Two larger silicates, a Fo_{97} olivine and a En_{96} low-Ca pyroxene, approximately ~0.5 μm in size were observed sandwiched between the large pyrrhotite grain and the fine-grained silicates.

The TP (Noni-A) from Track 58 (Noni) is shown in the

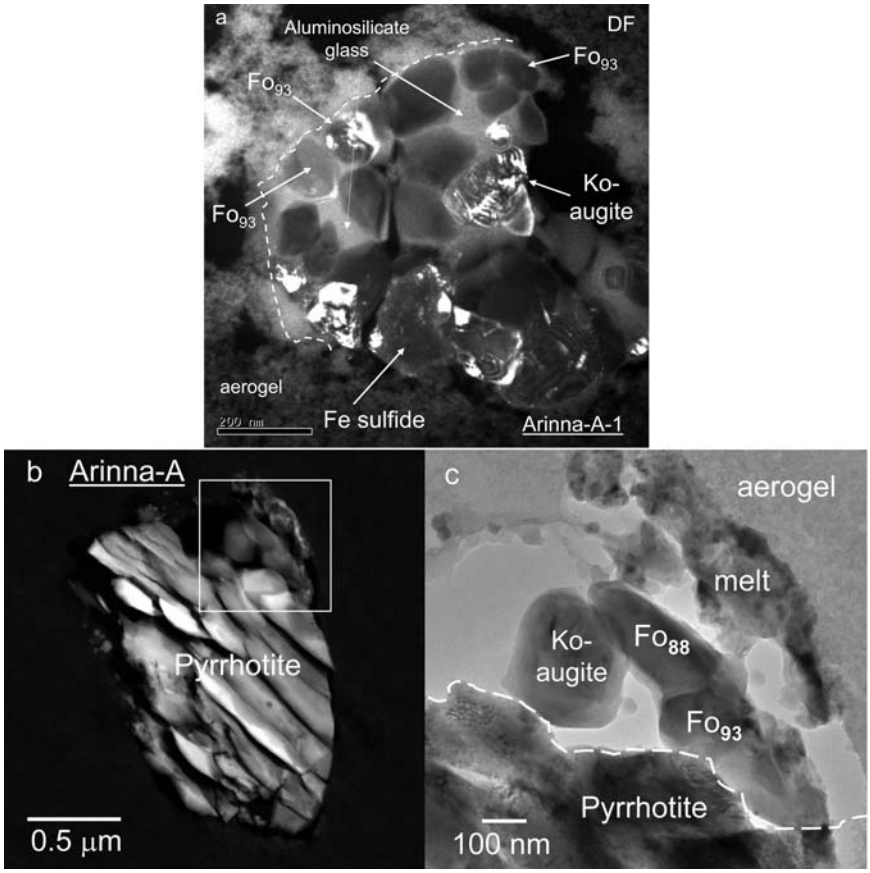

Fig. 3. a) Dark-field image of kosmochloric augite + FeO-bearing olivine + aluminosilicate glass assemblage Arinna–A-1 (Kool fragment), found isolated in aerogel. Similarity in mineralogy, grain sizes and textures to material attached to pyrrhotite TP shown in 3b and c suggest that this Kool grain was part of the same fragment prior to impact with aerogel. Fe-sulfide shown at the bottom of the figure is similar in composition to TP pyrrhotite further indicating that it was joined to the larger pyrrhotite shown in Fig. 3b. b) HAADF image of microtomed slice of large pyrrhotite grain and remnant Kool assemblage from track 10 (Arinna). c) Detailed bright-field image of Kool fragment minerals (kosmochloric augite + FeO-bearing olivines) attached to rim of pyrrhotite. Dashed line defines contact between remnant Kool grain and large pyrrhotite. Ko = kosmochloric, Fo = forserite.

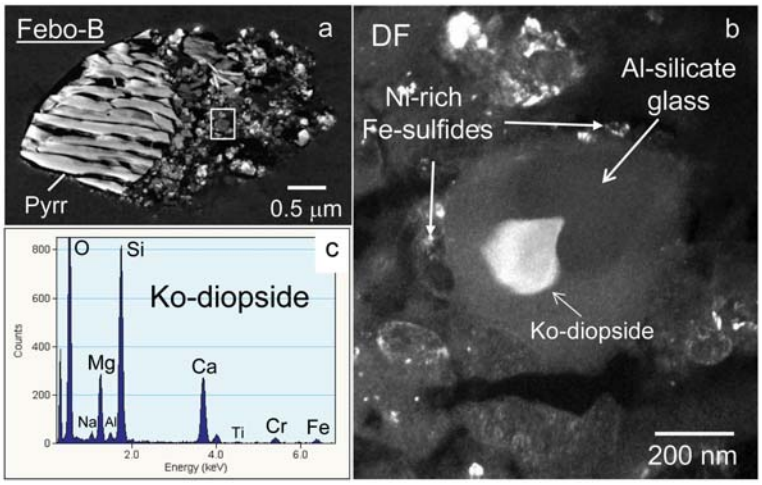

Fig. 4. a) HAADF image of TP Febo-B showing large pyrrhotite grain and attached fine-grained ~chondritic material. Single 0.5 μm Fo_{97} and En_{97} grains are present between the large pyrrhotite and the fine-grained material near the top of the figure but are probably not petrologically related to the Ko-diopside shown in (b). b) Magnified conventional DF image of the rectangular region in (a) showing diffracting Ko-diopside with attached Al-silicate glass and perimeter region containing Ni-rich Fe-sulfides. c) EDX spectrum of Ko-diopside shown in (b). Na_2O and Cr_2O_3 contents are 0.9 and 2.09 wt%, respectively.

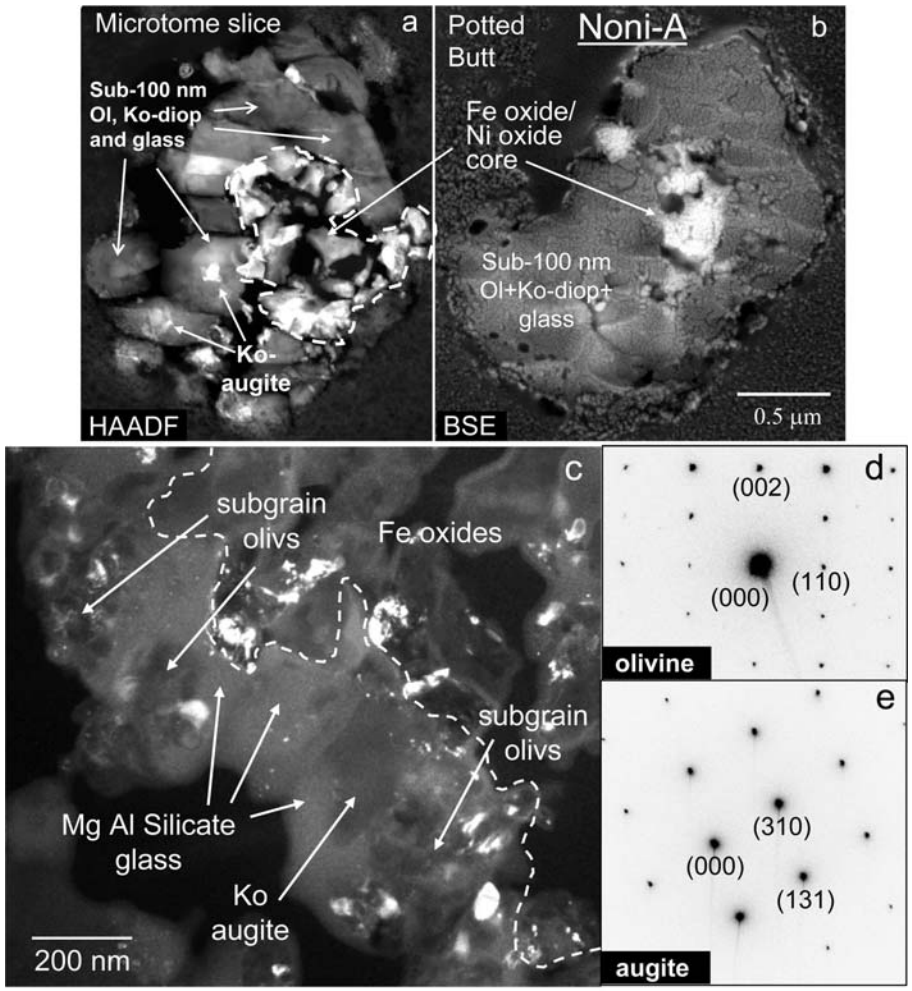

Fig. 5. Complementary images of microtome slice and potted butt from fragment Noni-A. a) HAADF image shows a complex mixture of <100 nm olivine and Ko-bearing diopside grains with silicate glass forming a thick shell around a central core of Fe oxides and Ni oxides outlined by the white dotted line. b) Backscatter FESEM image of the potted butt cut ~1 micron deeper into the fragment than the microtomed slice shown in (a). Central bright region shows Fe oxide and Ni oxide core. A small Fe-Ni metal oxide outlier is present on the left edge of the grain. c) Dark-field image of the interior of the microtome slice in (a). The figure shows a texturally complex mixture of olivine subgrains occurring in clusters with Mg-Al silicate glass and a single kosmochloric augite. The edge of the Fe oxide (and Ni oxide) core is visible to the right of the white dotted line. d) [-110] zone-axis diffraction pattern taken on a small olivine grain which matches JCPDS olivine 7–74 (Bayliss et al. 1980). e) [1–38] zone-axis pattern from kosmochloric augite crystal showing reflections consistent with JCPDS augite pattern 24–203 (Bayliss et al. 1980).

HAADF and BSE images in Fig. 5a and 5b. TEM EDX analyses and dark-field imaging have shown that this unusual TP is composed of two mineralogically distinct regions. One region is a complex assemblage of olivine crystals (subgrains) in silicate-rich glass with occasional Ko-augite grains which form a 1 μm concentric shell on a 1 μm wide core of Fe oxides and Ni oxides. In the shell region numerous <100 nm anhedral olivine crystals in glass occur in high density clusters with occasional Ko-augite crystals up to 200 nm in size (Fig. 5c). Diffraction patterns confirm the olivine and augite crystal structures (Figs. 5d, 5e). The texture of the shell region is distinct from the mineralogically similar assemblages seen in Coki-A and Arinna-A-1 (Figs. 2b and 3a).

Coarse-Grained Fragments

Coarse-grained Kool fragments were observed in three tracks (Isis, Puki and Coki) and one IDP (U2-20A14). Ko-clinopyroxene assemblages without olivine were present in two tracks, Sitara and KeyA (Table 1). Unlike their fine-grained counterparts, glass is absent with the exception IDP1 and SD fragment Coki-B-3 which contains either poorly crystalline albite or glass. Individual mineral grain sizes are generally larger than ~1 μm.

A microtome slice of wall fragment Isis-B from Track 41 (Isis), with apparent size of 2 μm, is shown in Fig. 6a. FeO-rich olivine appears to be concentrically surrounding a 1 mm × 1.5 mm central grain of Ko-augite. The round profile

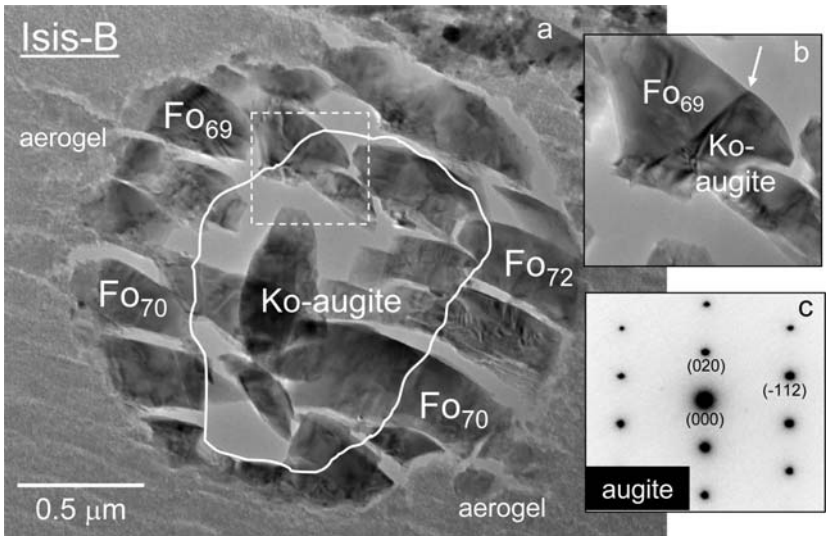

Fig. 6. a) Bright-field image of a microtome slice from coarse-grained fragment Isis-B, track 41. While solid line defines contact between FeO-rich olivine and Ko-augite. Spherical shape of fragment is from abrasion during aerogel capture. White interior regions are from separation or plucking of grains during microtoming. b) Magnified image of dotted box in interior of (a) showing sharp grain boundary contact between Fo_{69} and Ko-augite (arrow). c) SAED pattern obtained from augite shard on [201] zone axis. Angles and distances between reflections consistent with JCPDS augite 24–203 (Bayliss et al. 1980). Ko-augite = kosmochloric augite, Fo = forsterite.

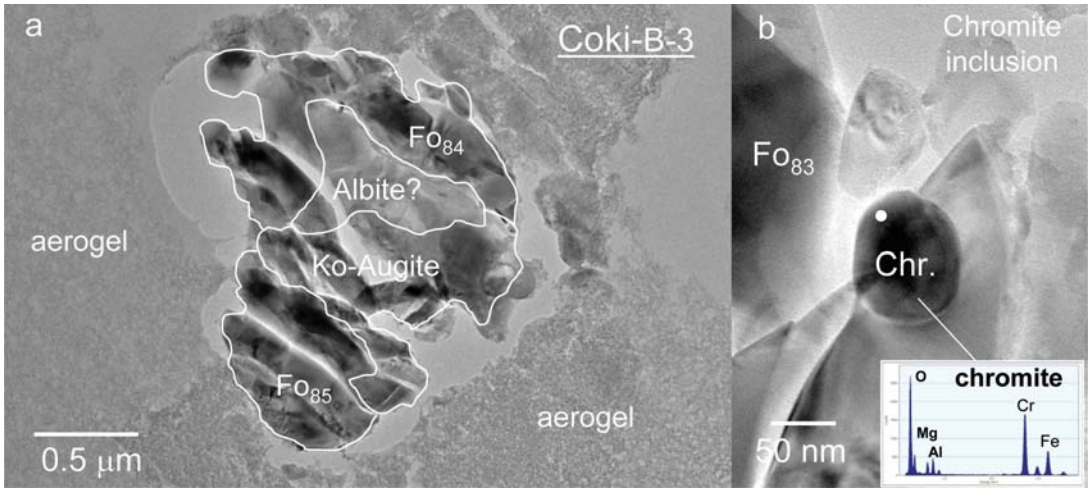

Fig. 7. a) Bright-field image of microtomed slice from fragment Coki-B-3, track 141. White outlines show extent of olivine, kosmochloric augite and albite/glass phase. b) Chromite inclusion from the interior of FeO-bearing olivine from an adjacent microtomed slice. Chromite is poikilitically enclosed in the olivine but appears on the edge of the shard as a consequence of microtoming. EDX spectrum taken from the upper left-hand edge of chromite grain (white dot) to minimize spectral peaks from enclosing olivine. Small unlabeled peaks in EDX spectrum are Fe_L, Si, $Cr_{K\beta}$, $Fe_{K\beta}$. Fo = forsterite, Chr = chromite, Ko = kosmochloric.

of the fragment is not due to melting but is a result of rounding from abrasion during collection in aerogel.

A second coarse-grained Kool fragment (Coki-B-3), from track 141, is composed of Fo_{85} olivine, Ko-augite and Na+Al-rich silicate glass or albitic feldspar all in sharp contact. We examined multiple microtome sections of this fragment and observed occasional round Cr-rich spinel inclusions up to ~100 nm in size in the olivine (Fig. 7b).

Backscatter FESEM potted butt and oriented BF images of a microtome slice of a >5 μm fragment from track 77 (Puki-B) are shown in Fig. 8. TEM EDX spectra collected from this microtome section and adjacent slices show that fragment Puki-B is composed of FeO-rich olivine, Ko-augite or diopside and a Na-Al silicate phase. Diffraction contrast observed in portions of this phase during tilting experiments suggest that it may be partially crystalline (transitional to albite). Pentlandite and a Ni-bearing Fe-sulfide occur as bright ~0.5 μm grains in the potted butt image (Fig. 8a). Surface textures visible in the BSE image along with TEM EDX analyses and imaging indicate that olivine, Ko-augite/

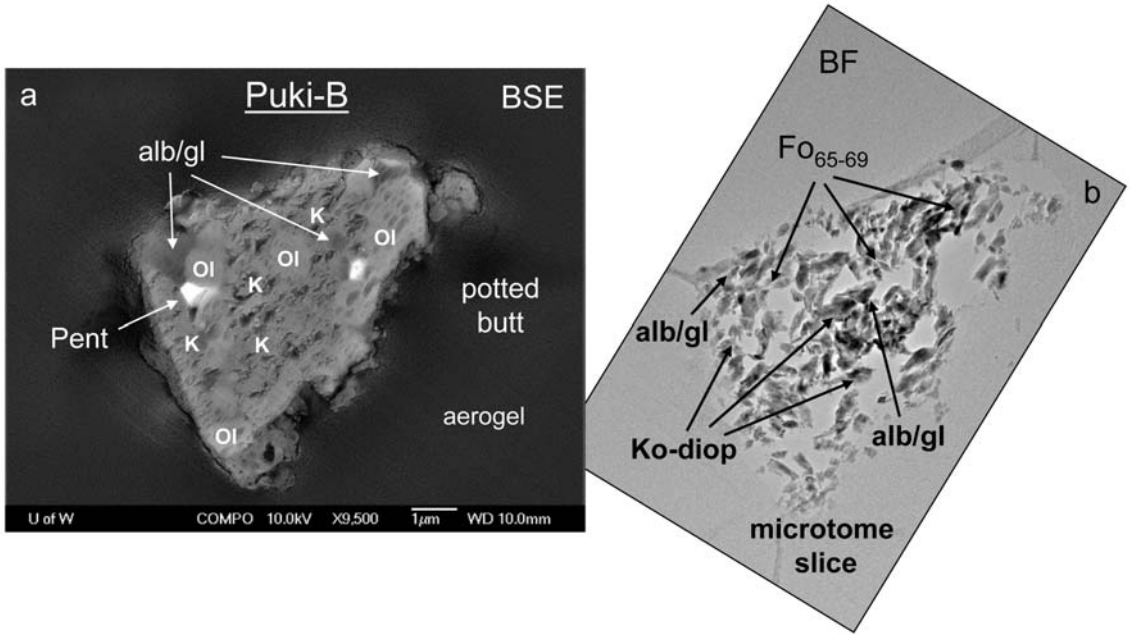

Fig. 8. Backscatter SEM image of potted butt and oriented complementary bright-field TEM image of microtome slice of large fragment Puki-B from track 77. a) Surface textures produced from microtoming show grain boundary relationships between kosmochloric diopside, olivine and albitic feldspar/glass. b) Microtome slice showing some identified shards of phases visible in (a). Lighter regions between shards indicate that significant plucking and some redistribution of grains occurred during cutting. Ol = olivine, Ko-diop = kosmochloric diopside, alb/gl = albite/glass, Pent = pentlandite. K = kosmochloric diopside.

diopside and the albite/glass phase are intimately mixed and generally homogeneously distributed throughout the fragment (Fig. 8a). Mineral grain sizes are typically >1 μm.

Kosmochloric augite is present in the TP of Track 27 (Sitara) in sharp contact with a large FeO-rich enstatite crystal (Fig. 9). Olivine is absent. On one end of the fragment a euhedral crystal of pentlandite with an apparent size of 1 μm is sandwiched between the FeO-rich enstatite and Ko-augite, while on the opposite end of the fragment a pyrrhotite grain >1 μm with a distinct curvilinear boundary is in contact with Ko-augite and a small region of FeO-rich enstatite. These features can be seen in the BSE image in Fig. 9a where surface textures and gray-level brightness easily differentiate these phases. The Ko-augite grains visible in two distinct locations of the fragment were apparently part of a larger single crystal which may have undergone plucking and size reduction from abrasion during capture. The scalloped surface textures present in all phases are a result of ultramicrotomy and are not primary features, but do provide important clues on the nature of the phase relationships which are not always obvious in the microtome sections. The FeO-rich enstatite crystal with its apparent size of 6 μm is one of the largest single mineral grains we have seen in all 16 Stardust tracks.

Mineralogically, perhaps the most unusual fragment containing Ko-clinopyroxene is the TP from track 56 (KeyA). This >5 μm fragment is modally dominated by the mineral roedderite (Zolensky et al. 2006; Joswiak et al. 2005), a ferromagnesian Al-poor alkali silicate (Fig. 10). Tilting experiments have shown that this phase is crystalline though parts, particularly along the fragment edges, appear to be poorly crystalline or even amorphous. Fe-free enstatite is the second-most abundant mineral in the fragment. Smaller amounts of Ko-bearing calcic pyroxene with Ca contents transitional between augite and pigeonite are found in contact with roedderite and enstatite. Initially identified as the amphibole richterite (Joswiak et al. 2007; Zolensky et al. 2006), additional analyses have shown that this phase is probably Ko-bearing augite/pigeonite. Diffraction patterns (Fig. 10) have shown that this phase is consistent with the JCPDS augite pattern 24–203 (Bayliss et al. 1980) rather than richterite amphibole.

Interplanetary Dust Particles

After observing that half of the examined SD tracks contain Ko-bearing calcic pyroxenes we revisited our mineralogical database on stratospheric IDPs and were surprised to find four contain Kool grains. A dark-field image of a microtomed slice from the interior of a chondritic porous interplanetary dust particle (IDP2) with submicron Ko-augite and FeO-rich olivine crystals and interstitial Al-silicate glass is shown in Fig. 11. Mineralogically and texturally, this IDP Kool grain is similar to the fine-grained SD Kool fragments discussed above. A 200 nm crystalline Na-Al silicate, probably albite-rich feldspar, was also found sandwiched between Fo_{77} and Ko-augite. Initial examination of this grain in the TEM indicated that it was crystalline, however, after a

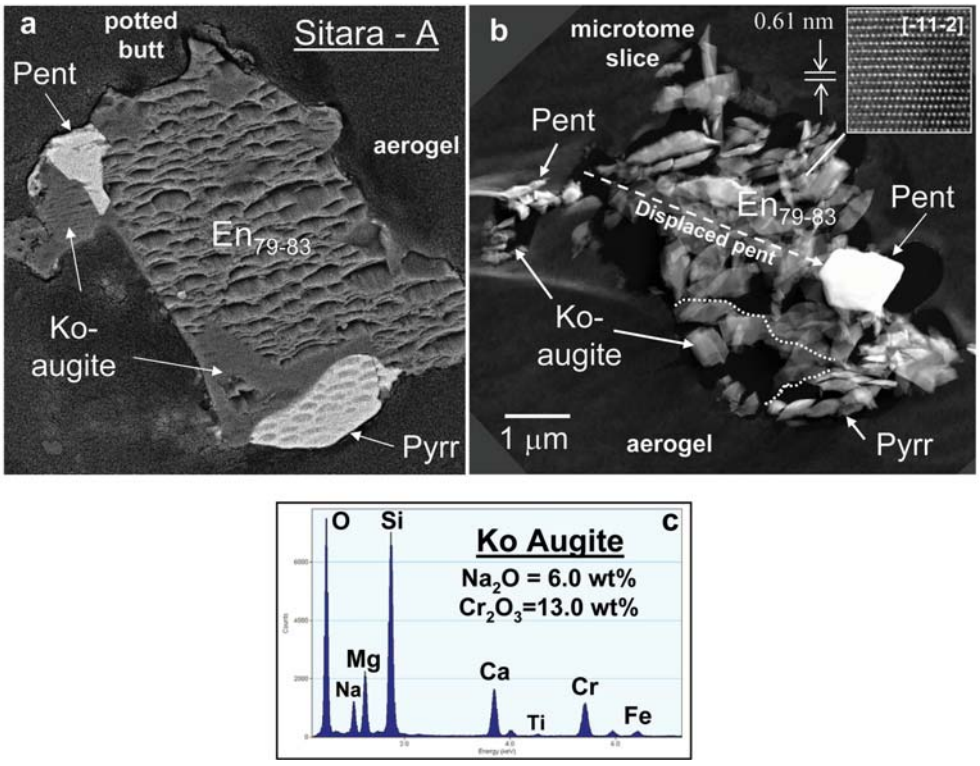

Fig. 9. Backscatter SEM image of potted butt and oriented complementary HAADF STEM image of microtome slice of TP Sitara-A from track 27. a) Surface textures from microtoming clearly delineate FeO-rich enstatite from two kosmochloric augite grains. Minor zone axis pattern [-11-2] is consistent with JCPDS clinoenstatite 19–769 (Bayliss et al. 1980). b) Microtome section cut approximately 1.6 microns above the potted butt. Dotted lines in lower right-hand side of figure delineate kosmochloric augite from enstatite and pyrrhotite. Large pentlandite grain displaced from original position during microtoming. c) EDX spectrum taken from Ko-augite shard. The Na and Cr contents in this Ko-augite are the highest of the observed Ko-clinopyroxenes in all fragments studied. En = enstatite, Ko-augite = kosmochloric augite, pent = pentlandite, pyrr = pyrrhotite.

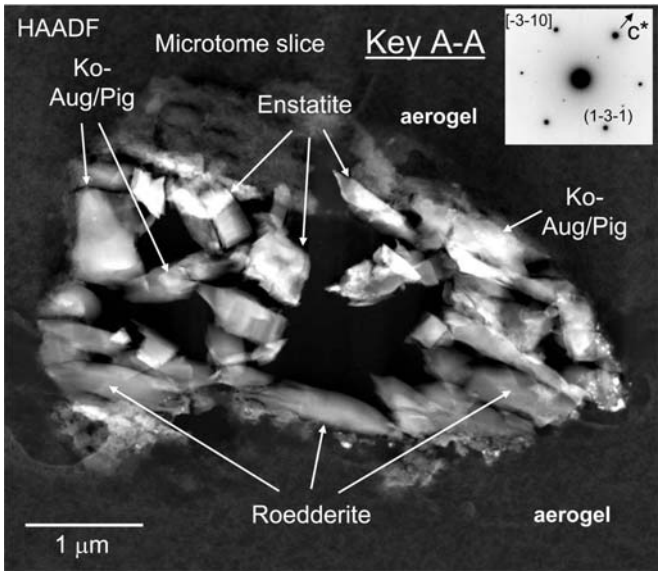

Fig. 10. HAADF image of microtome slice from fragment KeyA-A, track 56. Dark regions in center part of grain from plucking. Minor zone-axis diffraction pattern consistent with JCPDS augite 24–203 (Bayliss et al. 1980). Olivine is absent from this TP. Ko-aug/pig = kosmochloric augite/pigeonite.

short beam exposure the crystal suffered significant Na loss and amorphization, and we were unable to obtain a true composition or diffraction pattern of the grain.

Kool grains were also observed in the stratospheric IDP3 (U2073B-4F, Fig. 12). This chondritic porous IDP is approximately 5 μm in size and contains subgrains of Ko-augite, $Fo_{69–75}$ olivine and Al-silicate glass. An EDX spectrum of the pyroxene shows that the Na and Cr contents are high; we measured Na_2O = 2.6 wt% and Cr_2O_3 = 5.0 wt%. Unlike IDP2 in which glass occurs interstitially between crystalline grains, the Al-silicate glass in IDP3 tends to occur in regions up to 0.3 μm in size. Single crystals of Fe-sulfide and a Fe-Ni-Cu sulfide are also present. Much of the IDP was plucked during microtoming so we cannot be sure if additional phases were associated with these grains.

Small amounts of Na + Cr-rich augite were observed in IDP1 (U2-20A14, Table 1) and associated with equilibrated FeO-rich olivine. Abundant Mg + Al + Fe (minor K) silicate glass occurs in sharp contact with the olivine. Rare, rounded chromite-rich spinels up to 100 nm are poikilitically enclosed in the olivine. Because of significant sample loss and grain shattering during microtoming we cannot be certain of the grain sizes in this IDP, but it appears from the largest shards

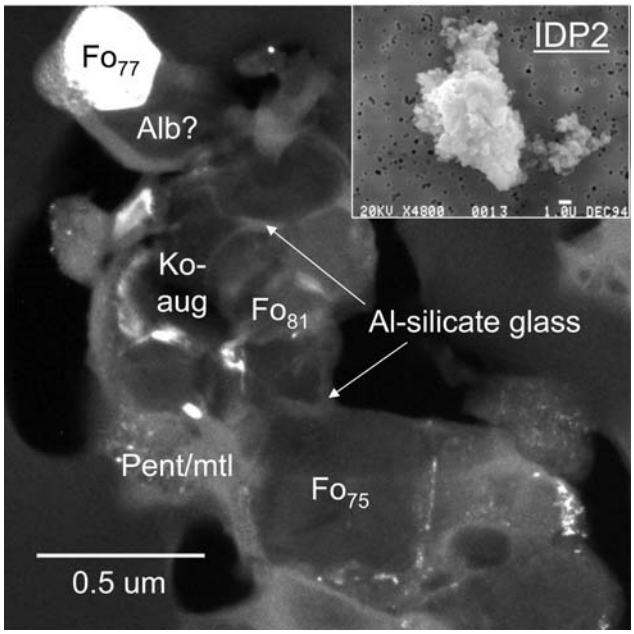

Fig. 11. Dark-field image of microtome slice showing mineralogically complex portion of IDP2 (U2073A-9A) containing submicron FeO-rich olivines, kosmochloric augite, interstitial Al silicate glass, and probable albitic feldspar (Kool grain). Relatively narrow range of olivine compositions suggests equilibration of this phase. Inset shows secondary electron image of entire stratospheric IDP. Ko-aug = kosmochloric augite, Fo = forsterite, alb = albite, pent/mtl = pentlandite/metal.

that olivine and Ko-augite grains are >1 μm indicating that IDP1 is coarse-grained and therefore texturally distinct from the other IDPs.

A fourth IDP (SP75), removed from a much larger cluster IDP and crushed between glass slides, also contains fine-grained Kool assemblages (Table 1) consisting of Ko-augite, FeO-rich olivine ($Fo_{77–83}$), probable albitic feldspar and aluminosilicate glass. Ni-bearing Fe-sulfides, magnetite and an unidentified Na-Fe-Mg phosphate are also present. Measured Na_2O contents of the Ko-augites, range from 2.80–3.25 wt%; these grains are typically subhedral in shape and <0.5 μm in size. A crystalline Na-Al silicate phase was observed in multiple locations, often with FeO-rich olivine. D-spacings measured from a diffraction pattern on a minor zone axis were consistent with albite XRD diffraction data file 10–393 (Bayliss et al. 1980) though one angular measurement between reflections was slightly larger than the expected value.

Unadorned mineral drawings produced from microtome sections of eight SD fragments and two IDPs containing Ko-clinopyroxenes are shown in Fig. 13. The drawings are grouped into coarse- and fine-grained assemblages and show that olivine, when present, is always in contact with Ko-augite suggesting coevolution of these phases. We note that IDP2 and IDP3 have similar textures and mineralogy as the fine-grained SD Kool fragments, Coki-A and Arinna-A-1.

Mineralogy and Mineral Chemistry

Ko-Clinopyroxenes

We measured the compositions of >30 clinopyroxenes from 8 SD tracks and 4 chondritic porous IDPs. Representative compositions are provided in Table 2 and a plot of all analyses is shown in the pyroxene quadrilateral in Fig. 14. Most clinopyroxenes fall toward the Mg-rich side of the augite and diopside fields; exceptions are the three analyses from fragment KeyA-A which fall in the sub-augite and pigeonite portions of the quadrilateral. These grains are significantly richer in Fe than the other pyroxenes. Several analyses of low-Ca pyroxene from SD fragment Sitara-A, shown as solid circles, fall in the enstatite field. Wo contents are moderately variable amongst the clinopyroxenes; in some fragments such as Puki-B, Wo variation is small while larger variations are observed in other fragments such as Arinna-A-1 (Wo = 32.1–49.2 mol%). IDP2 has the largest variability of the IDPs spanning a range from 32.7–46.6 mol% Wo and falling into both the diopside and augite fields. Ferrosilite contents have moderate variability within individual SD fragments. Fs contents in Arinna-A-1, for example, span a range from 27.6–37.6 mol%. In Sitara-A, the clinopyroxene Fe/Mg ratios are more tightly clustered (Fs = 3.5–5.7 mol%). A relatively large variation in Fs content is observed in IDP2 with Fs of 1.1–11.5 mol%. The quadrilateral shows that there is complete overlap between the SD and IDP pyroxenes.

All clinopyroxenes in the SD fragments and the four IDPs discussed in this paper are relatively rich in the elements Na and Cr. In the SD fragments, Na_2O and Cr_2O_3 contents range from 0.7–6.0 wt% and 1.4–13.0 wt%, respectively while in the IDPs, Na_2O = 2.2–3.3 wt% and Cr_2O_3 = 4.4–5.8 wt%. For comparison, the oxide wt% of Na_2O and Cr_2O_3 listed for 19 representative clinopyroxenes in chondrules from chondrites have maximum Na_2O and Cr_2O_3 contents of 0.69 wt% and 2.93 wt%, respectively (Brearley and Jones, 1998); these values are 3.9× and 1.5× lower than the average values observed in the SD pyroxenes, respectively.

A measure of the amount of kosmochlor component in the SD and IDP calcic pyroxenes is shown in the Na-Cr-Ca ternary plot in Fig. 15a. The figure illustrates the extent of mixing between diopside and kosmochlor endmembers and corresponds to a range of 5.0–39.9 mol% kosmochlor component (Table 2). Two additional characteristics are evident in the ternary plot. First, pyroxenes from single fragments in the SD tracks and the IDPs do not plot in tight clusters but show a wide range of solid solution between diopside and kosmochlor components indicating a wide compositional spread in Na, Cr and Ca. Pyroxenes from SD fragment Isis-B, for instance, shown as solid triangles, contain from 6.7–14.9 mol% kosmochlor component, a factor of >2× variation. A second characteristic evident from the plot is a small offset from the diopside-kosmochlor mixing

Table 2. Representative EDX analyses of kosmochloric clinopyroxenes (normalized wt% oxides).

Track/IDP	10	27	41	56	57	58	77	77	141	141	IDP1	IDP2	IDP3	IDP4
Name	Arinna- A-1	Sitara-A	Isis-B	KeyA-A	Febo-B	Noni-A	Puki-A	Puki-B	Coki-A	Coki-B-3	U2-2014A	U2073A-9A	U2073B-4F	U220:SP75
Ref.	244	150	155	359	183	223	121	131	434	365	396	416	424	463
SiO_2	57.01	52.96	51.31	54.60	58.05	56.44	56.35	53.29	53.37	53.50	53.18	55.56	53.82	55.81
TiO_2	0.53	0.96	0.35	b.d.	b.d.	0.28	0.25	0.46	0.29	0.59	0.77	0.23	0.81	0.67
Al_2O_3	1.89	0.62	0.67	0.06	0.65	0.46	0.53	0.39	1.05	1.84	0.73	0.59	1.00	0.70
Cr_2O_3	4.71	10.28	3.61	7.26	2.09	3.72	1.43	2.54	4.62	1.55	4.85	4.38	5.76	5.06
FeO	1.94	2.47	9.78	13.60	1.95	5.83	6.73	5.22	4.17	4.35	6.52	2.04	3.65	4.74
MnO	0.36	0.17	0.39	1.73	0.35	0.38	0.17	0.21	0.22	0.52	0.28	0.30	0.05	0.51
MgO	12.77	12.97	17.63	11.82	15.47	15.91	14.18	13.28	14.88	18.17	13.52	16.26	13.61	14.73
CaO	18.67	14.01	14.63	7.16	20.40	15.19	19.36	22.24	18.63	18.80	17.06	18.48	16.80	14.54
Na_20	2.13	5.54	1.63	2.90	0.90	1.78	1.00	2.37	2.78	0.68	3.07	2.16	3.34	3.25
K_2O	b.d.	b.d.	b.d.	0.86	0.13	b.d.	b.d.	b.d.	b.d.	b.d.	b.d.	b.d.	b.d.	b.d.
						Cations per 6 oxygen anions								
Si	2.05	1.95	1.92	2.05	2.08	2.05	2.06	1.98	1.94	1.95	1.97	2.01	1.96	2.03
Al	0.08	0.03	0.03	0.00	0.03	0.02	0.02	0.02	0.04	0.08	0.03	0.03	0.04	0.03
Cr	0.13	0.30	0.11	0.22	0.06	0.11	0.04	0.07	0.13	0.04	0.14	0.13	0.17	0.15
Ti	0.01	0.03	0.01	0.00	0.00	0.01	0.01	0.01	0.01	0.02	0.02	0.01	0.02	0.02
Mg	0.68	0.71	0.98	0.66	0.83	0.86	0.77	0.74	0.81	0.99	0.75	0.88	0.74	0.80
Fe(tot)	0.06	0.08	0.31	0.43	0.06	0.18	0.21	0.16	0.13	0.13	0.20	0.06	0.11	0.14
Mn	0.01	0.01	0.01	0.06	0.01	0.01	0.01	0.01	0.01	0.02	0.01	0.01	0.00	0.02
Ca	0.72	0.55	0.59	0.29	0.78	0.59	0.76	0.89	0.73	0.73	0.68	0.72	0.66	0.57
Na	0.15	0.40	0.12	0.21	0.06	0.13	0.07	0.17	0.20	0.05	0.22	0.15	0.24	0.23
Fs	7.8	9.6	23.7	34.1	6.6	17.0	21.0	18.1	13.6	11.8	13.1	6.6	13.1	15.3
Wo	49.2	41.2	31.3	19.3	47.0	36.3	43.7	49.6	43.7	39.6	43.5	43.3	43.5	37.5
Di	82.9	65.2	81.0	54.4	92.6	82.5	91.4	86.2	78.7	93.9	76.7	85.0	73.6	71.2
Ko	15.4	34.3	14.9	39.9	7.0	14.9	5.0	7.1	14.4	5.7	16.2	14.8	18.6	18.3
Jd	1.7	0.6	0.0	0.0	0.4	2.6	2.8	0.0	0.0	0.4	0.0	0.1	4.0	3.8
Ae	0.0	0.0	4.1	5.8	0.0	0.0	0.8	6.7	6.9	0.0	7.1	0.0	3.8	6.7

IDP = interplanetary dust particle, Fs = ferrosilite, Wo = wollastonite, Di = diopside, Ko = kosmochlor, Jd = jadeite, Ae = aegerine. b.d. = below detection.

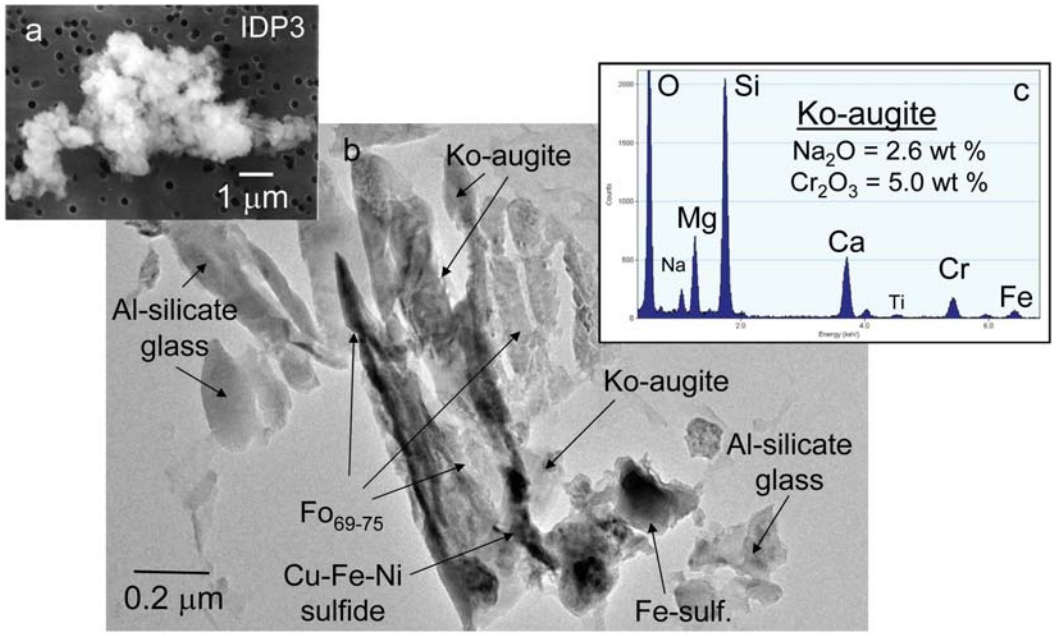

Fig. 12. a) Secondary electron image of chondritic porous IDP (IDP3: U2073B-4F) which contains kosmochloric augite. b) Bright-field image of microtomed slice of portion of the interior of IDP showing relationships between Ko-augite, FeO-rich olivine and other phases. c) EDX spectrum of kosmochloric augite. Note high Na and Cr contents.

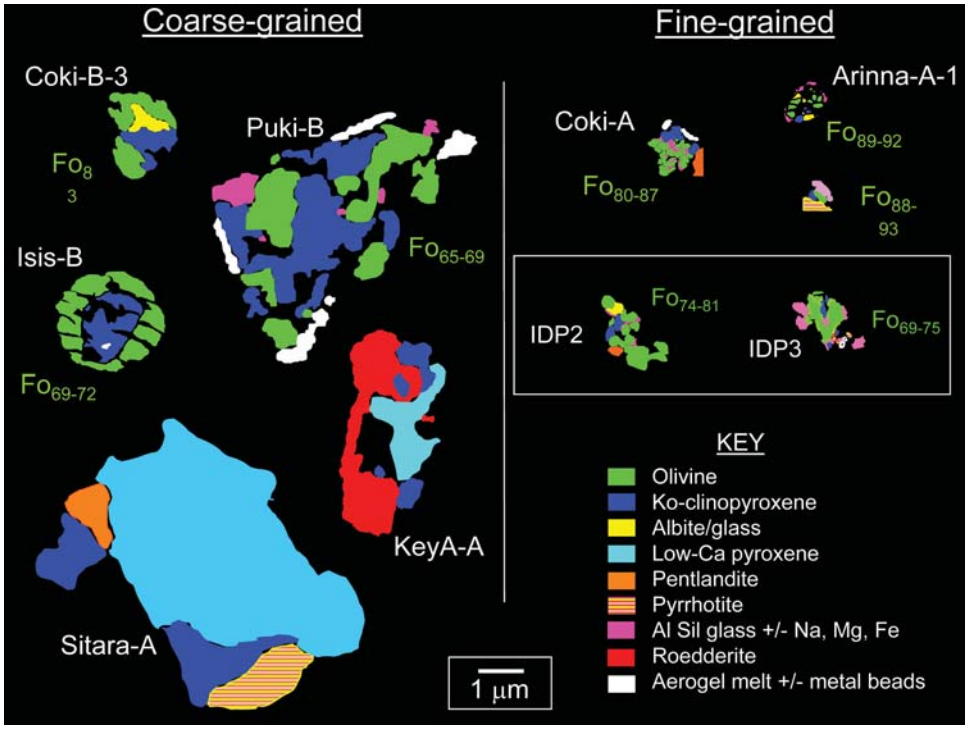

Fig. 13. Comparison of mineralogy and grain sizes of microtomed sections of Ko-bearing fragments studied from six SD tracks and two IDPs. The maps were not produced by conventional element mapping but rather by detailed examination of each microtomed section using a combination of EDX, imaging and tilting experiments. The SD fragments and IDPs are divided into coarse- and fine-grained portions based on grain sizes larger and smaller than 1 μm, respectively. Kool fragments are those which contain Ko-clinopyroxene + FeO-rich olivines (green and dark blue) ± Cr-rich spinel ± aluminosilicate glass or feldspar. Fine-grained Coki-A fragment and lowest Arinna-A-1 fragment are attached to large sulfides which are shown truncated. One micron scale bar applies to all maps.

Table 3. Representative EDX analyses of olivines (normalized wt% oxides).

Track/IDP	41	10	77	77	141	141	IDP1	IDP2	IDP3	IDP4
name	Isis	Arinna-A-1	Puki-A	Puki-B	Coki-A	Coki-B	U2-2014A	U2073A-9A	U2073A-4F	U2-20:SP75
Ref	157	243	122	402	429	332	397	408	425	466
SiO_2	37.03	39.49	37.35	37.93	45.86	39.28	34.94	38.01	37.34	39.36
Al_2O_3	b.d.	0.28	0.15	0.06	b.d.	b.d.	0.12	b.d.	b.d.	0.12
Cr_2O_3	0.13	0.24	0.08	0.02	0.13	b.d.	0.05	0.09	b.d.	0.12
FeO	27.29	9.89	27.47	29.22	13.87	15.97	31.48	21.24	25.45	18.95
MnO	0.73	0.91	0.42	0.66	0.62	0.55	0.81	0.71	0.40	0.72
MgO	34.44	48.84	34.31	31.45	45.86	44.19	32.17	39.72	33.87	39.49
CaO	0.20	0.35	0.21	0.26	0.32	b.d.	0.14	0.23	0.23	0.32
P_2O_5	0.18	b.d.	b.d.	0.29	0.56	b.d.	0.30	b.d.	2.71	0.83
					Cations per 4 oxygen anions					
Si	0.99	0.98	1.00	1.02	0.97	0.99	0.96	0.99	0.98	1.01
Al	0.00	0.01	0.00	0.00	0.00	0.00	0.00	0.00	0.00	0.00
Cr	0.00	0.00	0.00	0.00	0.00	0.00	0.00	0.00	0.00	0.00
Mg	1.37	1.80	1.37	1.26	1.72	1.67	1.31	1.54	1.32	1.50
Fe	0.61	0.20	0.61	0.66	0.29	0.34	0.72	0.46	0.56	0.40
Mn	0.02	0.02	0.01	0.01	0.01	0.01	0.02	0.02	0.01	0.02
Ca	0.01	0.01	0.01	0.01	0.01	0.00	0.00	0.01	0.01	0.01
P	0.00	0.00	0.00	0.01	0.01	0.00	0.01	0.00	0.06	0.02
Fa	30.5	10.1	30.8	34.0	14.4	16.8	35.1	22.9	29.5	21.0
Tp	0.8	0.9	0.5	0.8	0.6	0.6	0.9	0.8	0.5	0.8

IDP = interplanetary dust particle, Fa = fayalite, Tp = tephroite. b.d. = below detection.

line toward Na indicating that Na slightly exceeds Cr and that additional trivalent cations, Al and/or Fe^{3+}, are required for charge balance. Calculated diopside, kosmochlor, jadeite and aegerine endmembers are given in Table 2. About half of the analyzed pyroxenes have small aegerine components. The presence of ferric iron in some of the clinopyroxenes is also suggested in Fig. 15b by data points which plot below the 1:1 Cr + Al versus Na trend line.

Olivine

Thirty-five EDX analyses from olivines in Kool grains were obtained from 9 separate SD fragments and four IDPs. Representative compositions are provided in Table 3. Fayalite contents span a range from 10.1–35.1 mol% indicating that the SD and IDP olivines associated with Kool augites are FeO-rich. Within single SD fragments and individual IDPs, the range of Fe/Fe + Mg ratios are small to moderate ($Fo_{80–87}$ in Coki-A, for example) suggesting that these minerals are relatively equilibrated. Moderately high MnO contents (up 0.91 wt%) were measured. No significant compositional differences are evident in olivines between coarse- versus fine- grained morphologies. A few olivines from SD fragments may contain trace amounts of NiO (<0.1 wt%). Tiny Ni peaks in the EDX spectra of these olivines were below detection limits.

In SD fragment Febo-B a large olivine grain with composition Fo_{97} is present in the fine-grained material but is not associated with Ko-diopside. Olivine is conspicuously absent in the coarse-grained fragments Sitara-A and KeyA-A and we note that both contain low-Ca pyroxene. It is possible that olivine is present in these fragments but has not been observed due to undersampling because of their coarse-grain sizes.

Silicate Glasses and Poorly Crystalline Albitic Feldspar

Of the phases studied in the SD fragments and IDPs, silicate glasses are perhaps the most difficult to analyze and interpret. In the SD fragments, interpretation difficulties are in large part due to the ubiquitous occurrence of silica aerogel melt that is present around the fragments. There are at least four possible origins for glasses in the SD fragments: 1) The glasses are indigenous to the fragments and therefore primary, 2) partial melting of low temperature silicate minerals occurred during capture, 3) molten silica aerogel was injected into the fragment interiors during deceleration, and 4) molten silica aerogel mixed with partially melted impacting fragments. Of particular interest to this study are the primary glasses. We used a combination of compositional and textural criteria to determine whether a particular glass was primary or secondary (produced during capture). Glasses located in the interiors of fragments which contain the Al were interpreted as primary glass. Other elements, typically Mg and Fe and the alkalies Na and K were often present in these glasses.

High quality glass compositions were often difficult to obtain due to the tendency of some SD glasses to degrade under the electron beam, even at low current densities. Representative EDX analyses of glasses from 7 SD fragments and 4 IDPs are given in Table 4. Several analyses in the table are from probable albitic feldspars which are transitional from poorly crystalline materials or glass. All glasses are high in SiO_2 with moderate to high levels of Al_2O_3 (3.1–29.9 oxide wt%) and contain smaller amounts of CaO (0.0–1.8 oxide wt%), FeO (0.0–5.5 oxide wt%) and MgO (0.0–7.5 oxide wt%). Except for the SD fragment Coki-B-3 and IDP4 (Table 4, refs 453 and 466) Na_2O glass contents are generally low in abundance

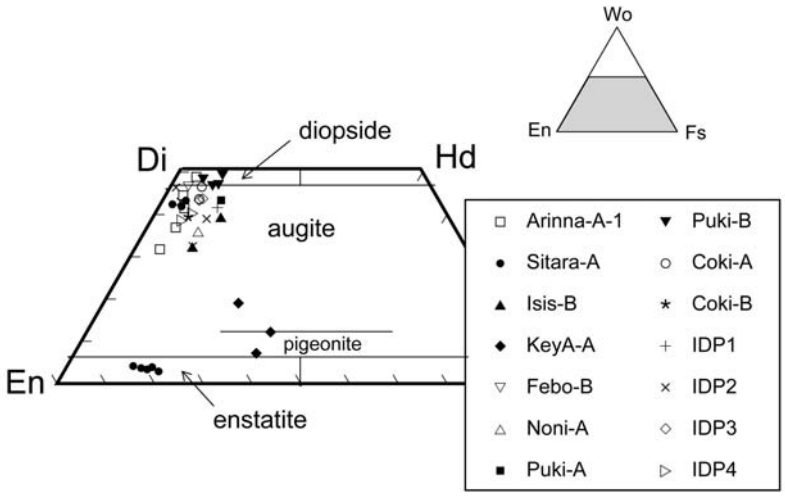

Fig. 14. Pyroxene quadrilateral showing the variation in pyroxene compositions measured in 10 SD fragments and 4 chondritic IDPs. Most of the Ko-bearing high-Ca pyroxenes plot on the Mg-rich side of the diopside or augite fields. Three pyroxene analyses from fragment KeyA-A plot in the subcalcic augite and pigeonite fields. Low-Ca pyroxene analyses from SD fragment Sitara-A are also shown in the quadrilateral.

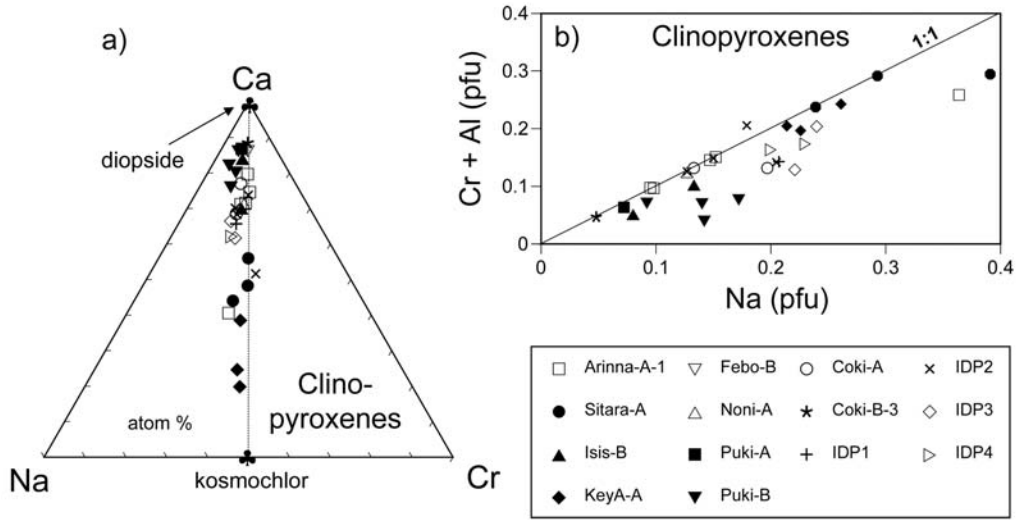

Fig. 15. a) Na-Cr-Ca ternary diagram (atom%) from 30 kosmochloric calcic pyroxenes observed in 8 SD tracks and 4 chondritic porous IDPs showing solid-solution between diopside and kosmochlor components. Offset in data points on Na-Ca side of ternary diagram indicates that Na > Cr (atomically) and that complex coupled substitutions must have occurred in the pyroxenes. b) Cr + Al versus Na scatter plot from SD and IDP Ko-bearing clinopyroxenes. Approximately half of the plotted pyroxenes fall beneath the Cr + Al versus Na 1:1 trend line indicating that additional cations are required to balance the excess Na. This suggests that ferric may be present in these pyroxenes as the compensating trivalent cation. Legend applies to both figures.

ranging from 0–2.9 wt%. The Na contents reported in the table should be regarded as minimums due to the high susceptibility of this element to volatilization. Aluminosilicate glass is readily seen in all the fine-grained SD fragments where it occurs interstitially with the Ko-clinopyroxenes and FeO-rich olivines (Figs. 2, 3a, and 5c). Aluminosilicate glass is also present in the four IDPs (Figs. 11 and 12), three of which have fine-grained textures similar to the fine-grained SD fragments (Fig. 13). Puki-B, a coarse-grained SD fragment, contains small amounts of Al-silicate glass (Fig. 13) with Na_2O contents up to 2.0 wt% (Table 4). Minor potassium (0.12–0.47 wt%) was present in most of the primary SD and IDP glasses.

Cr-Rich Spinels

Cr-rich spinels (chromite) are minor minerals found in at least four of the SD and IDP Kool grains. These minerals were observed as subhedral to partially euhedral inclusions in FeO-rich olivines (Fig. 7b) typically less than 200 nm in size. Compositions, given in Table 5, indicate that both the SD and IDP spinels are rich in the chromite endmember but also contain relatively high abundances of Mg, Al, Ti, and

Table 4. Representative EDX analyses of glasses and probable feldspars (normalized wt% oxides).

Track/IDP	10	27	58			141	141	IDP1	IDP2	IDP3U	IDP4	IDP4
name	Arinna-A-1	Sitara-A	Noni-A	77 Puki-B	141 Coki-A	Coki-B-3	Coki-B-3	U2-2014A	U2073A-9A	2073B-4F	U220: SP75	U220: SP75
Ref	248	154	227	442	439	453	365	398	423a	391	466	461
SiO_2	94.43	80.07	78.81	67.41	76.24	67.61	78.16	77.56	70.05	78.39	72.98	64.54
TiO_2	b.d.	b.d.	b.d.	b.d.	b.d.	b.d.	b.d.	0.17	b.d.	b.d.	b.d.	b.d.
Al_2O_3	3.13	7.25	14.73	29.11	13.62	20.14	19.23	7.08	24.95	19.37	18.64	29.93
Cr_2O_3	b.d.	b.d.	b.d.	b.d.	b.d.	b.d.	b.d.	b.d.	b.d.	b.d.	b.d.	b.d.
FeO	0.24	2.79	1.09	0.57	3.47	0.39	0.00	5.54	0.32	0.20	b.d.	1.73
MnO	b.d.	0.58	b.d.	b.d.	b.d.	b.d.	b.d.	0.32	b.d.	b.d.	b.d.	b.d.
MgO	0.48	7.55	4.12	0.32	4.16	b.d.	b.d.	8.04	b.d.	1.37	b.d.	1.77
CaO	0.34	0.29	0.47	0.16	1.10	0.25	b.d.	0.11	1.75	0.06	0.77	0.58
Na_2O	0.81	0.29	b.d.	1.96	0.19	11.18	2.13	b.d.	2.89	0.09	7.61	1.02
K_2O	0.28	0.12	0.40	0.47	0.42	0.42	0.47	0.25	b.d.	0.29	b.d.	0.43
P_2O_5	0.30	1.05	0.39	b.d.	0.81	b.d.	b.d.	0.93	b.d.	0.24	b.d.	b.d.
Normative minerals (mol%)												
Q	94.43	63.71	69.41	53.02	62.67	0.18	63.98	60.56	49.28	74.46	27.06	51.92
C	0.88	6.12	13.44	25.09	10.85	0.84	15.22	6.61	17.01	18.80	4.72	26.72
Or	1.65	0.71	2.36	2.78	2.48	2.48	2.78	1.48	0.00	1.71	0.00	2.54
Ab	6.85	2.45	0.00	16.59	1.61	94.60	18.03	0.00	24.45	0.76	64.40	8.63
An	1.69	1.44	2.33	0.79	5.46	1.24	0.00	0.55	8.68	0.30	3.82	2.88
Hy	1.55	23.95	11.85	1.63	15.42	0.57	0.00	28.42	0.47	3.70	0.00	6.91
Mt	0.05	0.62	0.24	0.13	0.77	0.09	0.00	1.22	0.07	0.04	0.00	0.39

IDP = interplanetary dust particle, Q = quartz, C = corundum, Or = orthoclase, Ab = albite, An = anorthite, Hy = hyperthesene, Mt = magnetite. b.d. = below detection.

Table 5. Representative EDX analyses of Cr-rich spinels (normalized wt% oxides)[1].

Track/IDP	77	141	IDP1	IDP2
Name	Puki-C	Coki-B	U2-20A14	U2073A-9A
Ref.	253	331	451	407
SiO_2	1.53	3.11	1.53	14.32
TiO_2	2.71	0.75	4.30	1.91
Al_2O_3	25.54	8.80	9.18	11.66
Cr_2O_3	27.84	54.96	47.86	39.14
FeO	38.06	24.07	24.39	19.37
MnO	0.09	0.71	1.13	0.98
MgO	3.76	6.96	11.50	12.89
CaO	b.d.	0.14	0.17	0.15
V_2O_3	0.48	0.51	0.75	0.57
Cations per 4 oxygen anions				
Si	0.05	0.10	0.05	0.43
Al	0.98	0.35	0.36	0.41
Cr	0.71	1.45	1.23	0.90
Ti	0.07	0.02	0.11	0.04
V	0.01	0.01	0.02	0.01
Mg	0.18	0.35	0.57	0.57
Fe	1.03	0.67	0.67	0.48
Mn	0.00	0.02	0.03	0.02
Ca	0.00	0.00	0.01	0.00
Olivine Host	Fo_{56}	Fo_{83}	Fo_{64}	Fo_{77}

[1]All spinel analyses include minor contributions from olivine hosts.
IDP = interplanetary dust particle. Fo = forsterite. b.d. = below detection.

V. Relatively large ranges of TiO_2 and V_2O_3 (0.75–4.30 wt% and 0.48–0.75 wt%, respectively) were measured. Charge balance calculations suggest that both divalent and trivalent iron is present; calculated $Fe^{3+}/(Fe^{2+} + Fe^{3+})$ ratios vary from 0.22 to 0.55.

Other Minerals

Large portions of the terminal particle KeyA-A are composed of a roedderite-eifelite solid solution ($(K,Na)_2Mg_5Si_{12}O_{30}$–$(K,Na)_3Mg_4Si_{12}O_{30}$) which is in direct contact with Ko-augite. Measured atomic Na/(Na + K) ratios vary from 2.2–3.8 and a maximum of 0.5 atom% Fe was found. Portions of this phase were poorly crystalline to amorphous, but generally were confined to the exterior of the fragment. This unusual SD fragment is mineralogically similar to some chondrules in ordinary chondrites (Krot and Wasson 1994; Wood and Holmberg 1994).

Bulk Compositions of Kool Fragments

Using a defocused electron beam and a long integration time we measured the bulk composition of the fine-grained fragment Coki-A which is composed of interstitial glass and >25 individual olivine and Ko-augite grains <200 nm in size (Fig. 2b). This fine-grained fragment is believed to most likely represent the bulk composition of Kool fragments. Major elements are plotted on the chondrite-normalized element/Si plot shown in Fig. 16 along with the bulk compositions from type II FeO-rich chondrules from ordinary chondrites (Lauretta et al. 2006; Kimura and Yagi 1979) and the average bulk composition of 11 Type II FeO-rich chondrules from the Semarkona meteorite (Jones 1990). The measured bulk composition from Coki-A is given in the table to the right of the plot. No measurements of the bulk

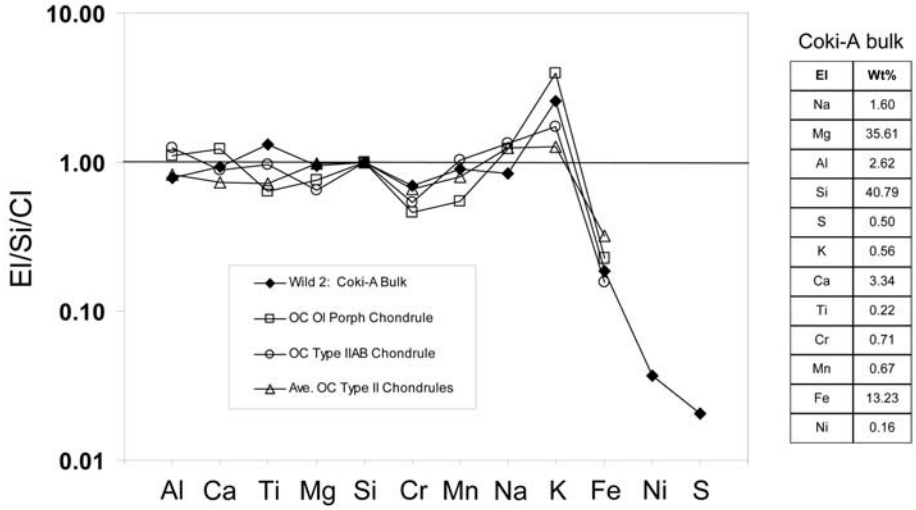

Fig. 16. Chondrite-normalized El/Si plot of bulk composition of the fine-grained Kool fragment Coki-A and type II FeO-rich chondrule compositions (bulk) from ordinary chondrites (Kimura and Yagi 1979; Jones 1990; Lauretta et al. 2006). The plot shows a similar pattern between the bulk composition of Coki-A and the chondrules. Depletions in Fe, Ni and S may suggest prior segregation of immiscible silicate and Fe-sulfide melts in Coki-A. The Kool fragment Coki-A is attached to a large Fe + Ni sulfide but does not contain fine-grained sulfides (See Fig. 2). Measured bulk composition of fragment Coki-A is provided on right-hand side of diagram (El wt%).

compositions of coarse-grained fragments were done as these are unlikely to be representative of the original impacting particles.

DISCUSSION

Previous Studies of Equilibrated Minerals in Anhydrous Interplanetary Dust Particles

A number of previous studies of chondritic anhydrous IDPs have shown that some contain Fe-bearing olivines and pyroxenes whose textures and mineral compositions are consistent with the assemblage forming at or near equilibrium conditions (Bradley 1994; Klöck and Stadermann 1994; Rietmeijer 1998; Keller and Messenger 2009). Described as equilibrated aggregates (Bradley 1994) or polyphase units (Rietmeijer 1998) these objects are composed of grains which vary between 100 nm and 0.1 μm that meet along well-defined grain contacts or form triple junctions. The Fe/Mg ratios between coexisting olivines and pyroxenes are correlated implying chemical equilibrium, at least with respect to Fe and Mg. Variable proportions of aluminosilicate or feldspathic glass are typically present. These characteristics are similar to the Kool grains discussed here but no compositions of clinopyroxenes have been reported thus we cannot be sure whether enhanced Na and Cr is present in these pyroxenes. Bradley (1994) suggests that the equilibrated aggregates may have formed by melting and subsequent recrystallization of pre-existing solid grains similar to chondrules in chondritic meteorites while Klock and Stadermann (1994) suggest that they may have thermal metamorphic or igneous origins (parent body).

Kool Grains Observed by TOF-SIMS

In addition to electron microscopy, TOF-SIMS studies also imply the presence of Kool grains in SD fragments. TOF-SIMS images, produced from secondary ions, show "hotspot" correlations between Na, Cr, Ca, and Mg that are consistent with kosmocholoric clinopyroxene (See figures 3 and 4, Stephan et al. 2008). Though not specifically identified as Ko-clinopyroxene by the authors, the high spatial correlation of these elements is a telltale sign of this phase due to its unusual composition. In the images, we interpret regions enriched in Fe, Mg and Mn which are immediately adjacent to the Ko-clinopyroxenes as FeO-rich olivine. High concentrations of nearby Al suggest that aluminosilicate glass or feldspar may also be associated phases. Thus, TOF-SIMS complement TEM and SEM techniques in identifying Ko-clinopyroxenes or Kool grains.

Igneous Crystallization versus Thermal Metamorphism in the Nebula

Stardust and IDP Kool fragment textures and mineral compositions support the idea that Kool grains formed either from silicate liquids or thermal metamorphism in the nebula and are unlikely to have originated from other processes such as condensation or shock heating. The evidence supporting igneous crystallization versus growth by thermal metamorphism is not entirely unambiguous however, and some fragments can be interpreted both ways. In the fine-grained Kool fragments, submicron grain sizes of the olivines and clinopyroxenes and interstitial glass suggest crystallization from silicate melts, possibly small droplets. Unlike many

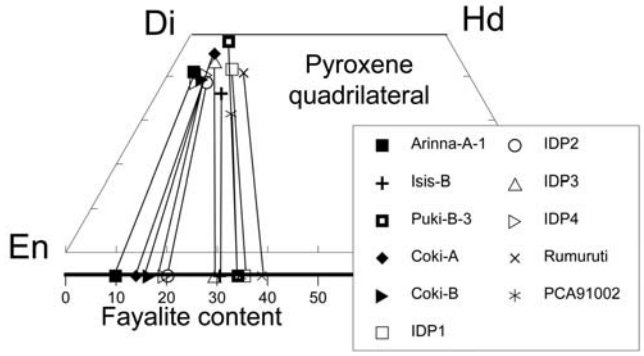

Fig. 17. Average compositions with connecting tie-lines of Ko-calcic pyroxenes and coexisting olivines in five SD fragments, 4 IDPs and recrystallized clasts or chondrule fragments in two R chondrites, Rumuruti and PCA 91002 (Schulze et al. 1994; Rubin and Kallemeyn 1994). Non-crossing tie lines suggest Fe-Mg cogenesis between pyroxene-olivine pairs. Number of analyses used in averages ranged from 1 to 5.

chondrules which have obvious spherical shapes implying formation from liquid melts in unrestricted environments, the external shapes of the primary SD particles are unknown due to physical modification during capture. If these fragments had formed by heating during metamorphism then we would expect the growth of larger grains as well as devitrification of the interstitial glass to feldspar as commonly observed in ordinary chondrites of the higher petrologic types (Huss et al. 2007). Rare incipient feldspars, transitional from glass, are observed in some of the coarser-grain Kool fragments (Table 1) suggesting thermal metamorphic origins for these particles. The presence of glass in the fine-grained Kool fragments is inconsistent with the relatively equilibrated Fe/Mg ratios in the olivines if these grains were produced by metamorphic heating.

Coexisting Ko-Clinopyroxenes and Olivines

The average compositions of Ko-clinopyroxenes and olivines from 5 SD fragments and 4 IDPs are shown in Fig. 17. Parallel tie-lines (with one exception) show that the Fe/Mg ratios between Ko-clinopyroxenes and coexisting olivines are correlated implying coevolution of these phases. Small to moderate variations in Fe/Mg ratios are observed in olivines from individual Kool fragments though pyroxene Fe/Mg ratios have a slightly wider variation (Fig. 14). Variable tie-line slopes imply that different Kool fragments formed under dissimilar conditions possibly related to changing fO_2 or bulk composition. For comparison, Na + Cr-bearing augites from equilibrated clasts or chondrule fragments from two R chondrites, Rumuruti and Pecora Escarpment (PCA) 91002 (Schulze et al. 1994; Rubin and Kallemeyn 1994) are also plotted (see below).

Trace and minor elements are often better indicators of petrogenetic history than major elements. If olivines and coexisting Ko-clinopyroxenes in the SD fragments and IDPs have a common evolution, such as in situ crystallization from liquids or reequilibration associated with thermal metamorphism, then we would expect partitioning of minor/trace elements to concentrate into their respective phases based on their known distribution coefficients. The minor elements that are in common to both the olivines and pyroxenes include Al, Ti and Mn. Experimentally determined D values for basaltic compositions (Becket et al. 2006; GERM Partition Coefficient Database, www.earthref.org/GERM/; Duke 1976) indicate that Al and Ti will preferentially partition into clinopyroxenes while Mn will show a slight preference for olivine. In Fig. 18 we plot measured apparent clinopyroxene-olivine partition coefficients ($D_{cpx/ol}$) from 5 SD fragments and 4 IDPs. In the figure Al and Ti plot above the D = 1 line indicating that these elements have partitioned into clinopyroxene. Conversely, the apparent partition coefficients for Mn plot below the D = 1 line indicating its preference for olivine. The figure demonstrates that the minor elements Al, Ti and Mn are concentrated into either olivine or clinopyroxene as expected from partition coefficient data providing evidence that olivine and Ko-clinopyroxenes are cogenetic. If the olivines and Ko-clinopyroxenes formed independently in different reservoirs or under open system conditions, it is unlikely that the partitioning of the minor elements between these phases would be so ordered.

Partitioning of Na and Cr into Kool Clinopyroxenes

Kool grain clinopyroxenes in this study have been shown to contain unusually high Na_2O (Table 2) while coexisting glasses are surprisingly low (Table 4). The Na_2O contents of Kool clinopyroxenes versus coexisting glasses are plotted in Fig. 19. Also plotted in the figure are clinopyroxene-mesostasis pairs from type II FeO-rich chondrules from ordinary chondrites (Alexander and Grossman 2005). Experimental clinopyroxene-glass distribution coefficients from basaltic systems range from about 0.04–0.25 (Henderson 1982; Mahood and Stimac 1990; Blundy et al. 1995; Lundstrom et al. 1998; Jones and Layne 1997; Huang et al. 2006; GERM partition coefficient database). D values are >1 for nearly all clinopyroxene-glass pairs from SD fragments and IDPs. An important question is why sodium is concentrated in the Kool pyroxenes rather than in the coexisting glasses if the glasses formed cogenetically. One explanation may point to the presence of Cr in the melt during crystallization of pyroxene. Distribution coefficients between crystalline phases and melt are complex functions of temperature, pressure, crystal and melt composition, and melt structure (Mysen and Virgo 1980; Mahood and Stimac 1990; Harlow 1996; Lundstrom et al. 1998; Huang et al. 2006). The presence of one element in a melt can dramatically affect partitioning behavior of the other, particularly during coupled substitutions. For instance, Karner et al. (2007) demonstrate that increased Cr^{3+} substitution into augite in synthetic Martian basalt results from increased availability of Na and Al cations in the melt phase

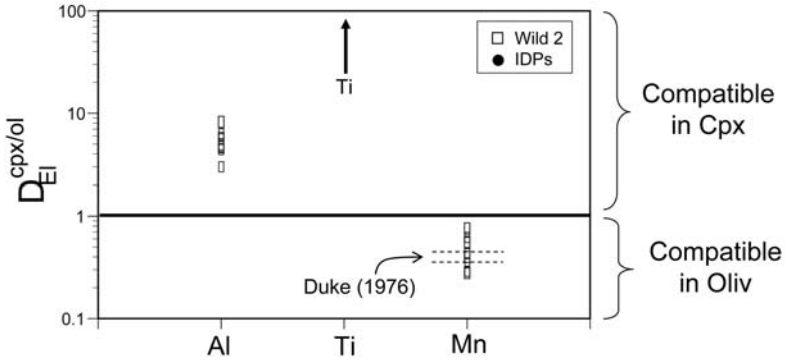

Fig. 18. Measured apparent partition coefficients for the elements Al, Ti and Mn between clinopyroxene and coexisting olivine in SD and IDP Kool fragments. Element Ti was below detection limits in all measured olivines thus arrow shows minimum apparent partition coefficient of 100 for this element. Plot shows that Al and Ti are more compatible in clinopyroxene and Mn is more compatible in olivine consistent with experimental partition coefficients for these elements (Becket et al. 2006; GERM Partition Coefficient Database, www.earthreforg/GERM/). Horizontal dotted lines around Mn data points show experimentally determined range of clinopyroxene/olivine distribution coefficients for this element from Duke (1976) experiments. El = element, cpx = clinopyroxene, ol = olivine.

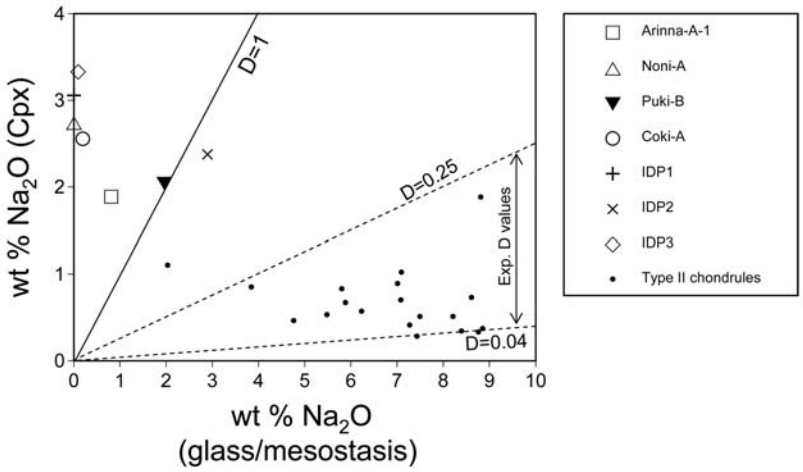

Fig. 19. Na_2O contents in Ko-clinopyroxenes and coexisting glasses in SD and IDP Kool fragments. The range of experimental clinopyroxene-melt distribution coefficients in basaltic systems is bracketed by the dotted lines at D = 0.04 and D = 0.25 (Henderson 1982; Mahood and Stimac 1990; Blundy et al. 1995; Jones and Layne 1997; Lundstrom et al. 1998; Huang et al. 2006; Lundstrom et al. (1998); GERM partition coefficient database). SD and IDP clinopyroxene-glass pairs plot considerably outside this range showing that significantly more Na is present in the SD and IDP clinopyroxenes relative to their coexisting glasses than predicted by experiments. This has lead to the hypothesis that the clinopyroxene distribution coefficients appropriate to the SD Kool grains are much higher than predicted in experiments because of coupled substitutions of Na and Cr into the clinopyroxenes (see text). Na loss in the glasses was also likely during EDX measurements. Solid dots show the distribution of clinopyroxene-glass pairs from type II FeO-rich chondrules in ordinary chondrites (Alexander and Grossman 2005).

due to delayed crystallization of plagioclase feldspar. Similarly, Lundstrom et al. (1998) (and references therein) showed that high field strength element concentrations (Ti, Zr, Nb, Hf, and Ta) increase in clinopyroxenes, relative to melt, by factors of 2–8× in the presence of tetrahedral Al, because of its charge-balancing role. In the Kool fragments, higher concentrations of Cr in the melt along with the charge-balancing cation Na may have effectively increased the partitioning of these elements into clinopyroxene.

Coupled substitutions also influence solid-solid partitioning via metamorphic exchange. In a study of a terrestrial chromian diopside containing up to 1.5 wt% K_2O, Harlow (1996) showed that the incorporation of Cr^{3+} into the M1 sites leads to expansion of the M2 sites facilitating entry of alkalis. Thus, the availability of the charge-balancing cation Cr^{3+} effectively increases the clinopyroxene-alkali distribution coefficients simply due to the presence of Cr^{3+}. Although the K-bearing diopside in the Harlow (1996) study was found as an inclusion in diamond and therefore formed at high pressures, Tsujimori and Liou (2005) observed K-rich Ko-diopsides in low pressure serpentinites showing that high pressures are not required for incorporation of alkalis in the pyroxenes. Thus, the availability of charge balancing cations during solid state re-equilibration may dramatically increase both Na and Cr in clinopyroxenes.

Other causes may also explain the high concentration of Na in the clinopyroxenes. For instance, Na abundances may have been much higher in the glasses in the past but were lost

during a heating event or perhaps the Kool fragments crystallized at high pressures where Na behaves compatibly. Both explanations are somewhat unsatisfactory. If Na in the glasses was lost during open system heating then the Na contents of the coexisting clinopyroxenes would have been unrealistically high for typical clinopyroxene-glass partition coefficients. Likewise, no high pressure phases or widespread shock effects in the Kool grains have been observed suggesting that high pressure formation was not a likely mechanism.

Crystallization of Fine-Grained Kool Fragments

We suggest that some of the Kool fragments (those that appear to have igneous origins) may have formed in situ from the crystallization of liquids in the nebula. To further study this we use the bulk composition measured from Kool fragment Coki-A (Figs. 2b and 16) and the 1-atm forsterite-diopside-albite liquidus ternary phase diagram shown in Fig. 20 (Schairer and Morimoto 1958). Although it is not certain whether Kool grains crystallized strictly under equilibrium conditions the use of the equilibrium diagram is never-the-less useful to explain how the clinopyroxenes may have become enriched in kosmochloric components. We note that the modal proportions of glass are relatively low and that the distribution of Fe and Mg and the minor elements Al, Ti and Mn between coexisting olivine and pyroxene are consistent with these phases crystallizing near equilibrium. The phase diagram applies strictly CaO-MgO-Al_2O_3-CaO (CMAS) compositions and does not consider Fe-bearing systems. FeO, however, constitutes <10% of the bulk composition of Coki-A. In the ternary diagram the bulk composition of Coki-A is shown as the solid circle near the forsterite apex and relatively close to a chondritic composition melt. A liquid droplet with a bulk composition similar to Coki-A and above its liquidus temperature will intersect the liquidus surface in the forsterite + L field crystallizing olivine as shown by the solid circle and indicated by the arrow for "Coki-A bulk". As the temperature falls and more olivine precipitates from the melt, the liquid is driven away from the forsterite apex as shown by the heavy arrowed line in the figure. In a system involving Fe, such as under discussion here, olivine of course, would incorporate this element as crystallization proceeds.

Chromite spinels are often early liquidus phases in terrestrial basaltic and ultramafic systems. (Barnes 1998). Chromite is only occasionally observed in the SD Kool fragments and it is always poikilitically enclosed in FeO-rich olivines consistent with early precipitation. When the forsterite-diopside cotectic is reached after continued falling temperature, the liquid is enriched in Si, Al, alkalies, Ca, Ti and Cr which constitutes approximately 24 wt% of the system. At this point diopside begins to coprecipitate with olivine. Feldspar crystallization has not yet begun and thus Na

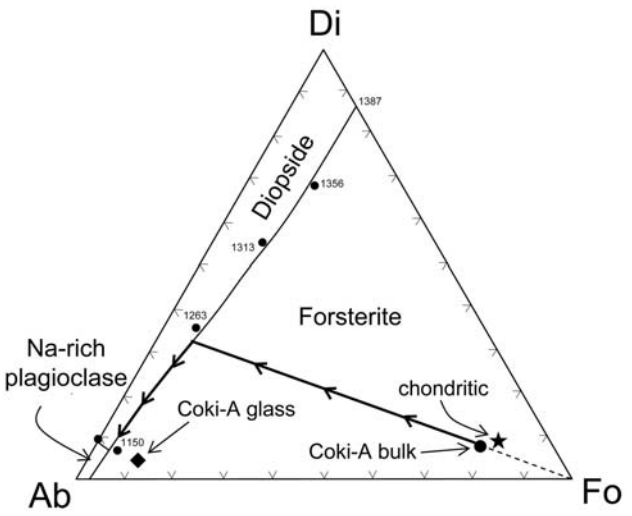

Fig. 20. 1-atm Fo-Di-Ab liquidus ternary phase diagram (Shairer and Morimoto 1958) showing possible equilibrium crystallization path in glass-bearing fine-grained Kool fragments. Diagram shows that cooling of a melt with bulk composition equivalent to Kool fragment Coki-A crystallizes forsterite (olivine), followed by diopside (clinopyroxene) and albitic feldspar (or Na-bearing aluminosilicate glass). Measured composition of Coki-A glass (solid square) is close to eutectic composition. Offset suggests that a small amount of olivine was present in the analysis. See text for detailed discussion.

and Cr, which exist at elevated levels in the liquid, are available for incorporation into clinopyroxene. It is not clear why chromite did not crystallize during this stage of cooling even though Cr was present at elevated levels in the melt. Chemical analyses of the interstitial glasses show that Kool grains are low in CaO which presumably indicates the incorporation of this oxide into clinopyroxene. With continued falling temperature and coprecipitation of diopside and olivine the liquid moves toward the Ab apex. Olivine and diopside are often seen in direct contact in the Kool fragments providing evidence of this cocrystallization (Fig. 3a). During this interval, Cr and Na in the melt phase continue to enter the precipitating clinopyroxene. We surmise that a "tug-of-war" between Cr which prefers clinopyroxene and Na which is more compatible in the melt, is occurring and that Cr entering into clinopyroxene prevails in the competition over Na being retained in the melt. Certainly, if Cr were not present in the melt phase, then little to no Na could enter clinopyroxene (although Al may play a small role in this system).

During late stage cooling the Al content of the residual melt is expected to increase since significant Al was not incorporated into diopside. The total amount of Na that is incorporated into diopside will depend on the modal abundance of clinopyroxene as a liquidus phase and the amount of Cr present in the melt. Thus, either albitic feldspar or aluminosilicate glass (with minor Na) will form. In most Kool grains low-Na silicate glass is observed though we have seen at least one SD fragment and one IDP with a Na-Al silicate phase with a composition that is equivalent to

stroichiometric albite. If feldspar crystallizes then the final composition will lie at the albite-diopside-forsterite ternary invariant point otherwise the liquid composition will move out of the ternary diagram. The 'invariant' point may either be a true invariant eutectic or the liquid may proceed along an albite-diopside cotectic toward a piercing point on the albite-diopside join. In either case, it doesn't significantly affect the final liquid composition as both points are spatially very close Experimental studies have shown that albite crystallization is problematic due to nucleation difficulties in high viscosity melts (Morse 1980; Okuno and Marumo 1982). The plotted composition of Coki-A glass (solid square) on the ternary diagram shows that it falls near the albite-diopside-forsterite eutectic (or near the piercing point) consistent with expected late-stage liquids. The displacement of the position of the Coki-A glass composition slightly off the eutectic may reflect that small amounts of olivine are present in the glass analysis due to experimental difficulties with obtaining a pure glass composition. From the positions of the bulk composition and the final crystallizing phases, the total solid composition should consist of a mixture of approximately 74 wt% olivine, 10 wt% diopside and 16 wt% albite (or Na + Al-bearing silicate glass). We note that in Kool grains olivine is modally dominant over both clinopyroxene and Al ± Na-bearing silicate glass (or poorly crystalline albite).

Comparison of Fine-Grained Kool Fragments to Type II FeO-rich Chondrules from Ordinary Chondrites

Type II PO chondrules in ordinary chondrites (Kimura and Yagi 1980; Jones 1990; Alexander and Grossman 2005) and fine-grained Kool grains have similar bulk compositions with respect to many major lithophile elements (Fig. 16). Both contain FeO-rich olivines, Cr-rich spinels and aluminosilicate glass (alkali-rich mesostases in the chondrules) while metal is absent or only present in minor quantities and both lack low-Ca pyroxenes. The chondrules, however, lack clinopyroxene phenocrysts though occasional small clinopyroxenes may be present in the mesostases (Jones 1990). Average fayalite contents of the chondrule olivines range from $Fa_{12–18}$ and individual grains are zoned from $Fa_{10–30}$. This compares to $Fa_{10–30}$ fayalite contents in fine-grained Kool fragment olivines. Cr-rich spinels are present in chondrules and Kool fragments but show differences in abundances and associated phases. In the Kool fragments Cr-rich spinels were infrequently observed and always found as inclusions in olivine unlike the chondrules where chromites are relatively numerous and often observed as large euhedral crystals. In the chondrules most of the Cr was partitioned into chromite.

Cr_2O_3 abundances in Kool grain olivines are lower (0.0–0.25 wt%) than in the chondrule olivines (0.38–0.51 wt%). Since most of the Cr in the Kool grains is locked up in clinopyroxene with some in chromite, this may account for its paucity in olivine. (Cr is also mildly incompatible in olivine relative to melt). In the chondrules, however, Cr was likely available in the melt for substitution into early crystallizing olivine because chromite precipitated toward the end of olivine crystallization. Thus, if the Kool grains crystallized from melts similar in composition to type II PO chondrules in OCs, then the minerals that crystallized (clinopyroxene) and their crystallization sequences were different. These differences may account for the high Cr and Na abundances in the Kool clinopyroxenes.

Kool grains, like the chondrules, do not show the alkali depletions that would be expected if these objects crystallized from high temperature melts in the nebula. With higher surface/volume ratios, evaporation in Kool grains should have been even higher than in chondrules under similar conditions. We have not satisfactorily been able to resolve this difficulty with Kool grains. We note that an inadequate solution to this problem with chondrules also exists. One recent idea suggests that high dust/gas ratios in the nebula provided an environment of equilibrium between evaporation and recondensation thereby maintaining alkali abundances (Alexander and Grossman 2005). Kool grains, which are frequently observed in the SD tracks and must have been abundant in the nebula, at least locally, may also have existed under a similar dynamic equilibrium state as the chondrules. Some of the preservation of Na in the Kool grains may be attributed to being locked into clinopyroxene thus reducing its mobility for volatilization. This would require that clinopyroxene be the earliest (or very early) precipitating phase during crystallization of the Kool melts, but this is not consistent with the observed textures in these fragments.

Comparison of Coarse-Grained Kool Fragments to R Chondrites

R chondrite meteorites are oxidized type 3 breccias (largely) containing equilibrated to unequilibrated chondritic lithic clasts, variable chondrule types, chondrule fragments and fine-grained matrix. Some of the members of this group include the Carlisle Lakes meteorites, Allan Hills (ALH) 85151 and Yamato (Y) 75302, (Weisberg et al. 1991), PCA 91002 (Rubin and Kallemeyn 1994), Acfer 217 (Bischoff et al. 1994), and the only known R group fall Rumuruti (Schulze et al. 1994). These meteorites are dominated by fine-grained matrix composed of FeO-rich olivines (2–3 μm in size), high and low Ca-pyroxenes, albitic feldspar and Cr-rich spinel and contain lower proportions of porphyritic ferromagnesian chondrules, chondrule fragments and equilibrated lithic clasts. Porphyritic olivine chondrules (and chondrule fragments) are the dominant chondrule type and are characterized by equilibrated FeO-rich olivines, Na + Cr-bearing clinopyroxene, albite-rich feldspar and minor chromite. These phases are also observed in lithic clasts and sometimes in matrix.

Coarse-grained Kool fragments are composed of >1 μm minerals and generally lack glass. These objects may have formed by thermal metamorphism in the nebula rather than igneous crystallization believed responsible for the formation of fine-grained Kool fragments. Here we compare the coarse-grained Kool fragments to recrystallized clasts and chondrules from R chondrites.

Large light recrystallized clasts in the Rumuruti chondrite contain modally dominant FeO-rich olivine (with Cr-rich spinel inclusions), augite/diopside with moderately high Na and Cr contents and albitic feldspar and lack low-Ca pyroxenes and metal, an assemblage nearly identical to the coarse-grained Kool fragments. The high Ca-pyroxenes range from subcalcic-augite to diopside and have relatively high Na_2O and Cr_2O_3 contents (0.56–0.81 wt% and 0.41–0.97 wt%, respectively) compared to clinopyroxenes from other chondrite groups (Rubin and Kallemeyn 1994; Schulze et al. 1994; Brearley and Jones 1998). FeO-rich olivine is often equilibrated around $Fa_{38–40}$ and plagioclase is typically albitic ($Ab_{0.89–0.96}$). The coarse-grained SD Kool fragment Coki-B-3 contains $Fo_{15–17}$ olivine, Ko-augite (Na_2O = 0.68 wt%, Cr_2O_3 = 1.55 wt%), poorly crystalline albitic feldspar and chromite. Glass is absent. Cr_2O_3 abundances in olivine are similar in R chondrites and coarse-grained SD Kool fragments. In PCA 91002 and Rumuruti, published Cr_2O_3 contents are 0.04 wt% and 0.11–0.19 wt%, respectively (Rubin and Kallemeyn, 1994; Schulze et al. 1994) while Cr_2O_3 contents in olivines from the SD and IDP coarse-grained Kool fragments are <0.13 wt%. Chromite inclusions are poikilitically enclosed in olivine in the Kool fragment Coki-B-3 and in olivine in R chondrites and are rich in Ti, Al, Mg and Mn in both materials. Average calculated ferric iron content in the Acfer 217 chromite is 15 wt% (Bischoff et al. 1994) compared to 3.3 wt% in chromite in Coki-B-3. Additionally, high FeO contents in the olivines and lack of metal show that both Kool grains and R chondrites formed in oxidizing conditions. The R chondrites appear to have formed via thermal metamorphism either on their parent body(ies) or in the nebula (Kallemeyn et al. 1996) and represent the end-member of an increasing oxidation trend from the ordinary chondrites, H → L → LL → R (Schultze et al. 1994). Glass is generally absent from these meteorites and sodic plagioclase may have formed from pre-existing albitic glass. Coarse-grained Kool fragments appear to have formed in high temperature oxygen-rich environments similar to R chondrites.

Comparison to Agglomeratic Chondrules

Fine-grained agglomeratic chondrules (Weisberg and Prinz 1996) from unequilibrated ordinary chondrites are somewhat analogous materials to Kool grains. These objects formed by incomplete melting of solid grains in the nebula and were suggested to be reasonable chondrule precusors. Similar materials were also discussed by Dodd (1971), Rubin (1984), and Van Schmus (1969). The agglomeratic chondrules are dominated by FeO-rich olivine grains <5 μm in size and some contain submicron olivines though larger grains up to 400 μm in size are also present. Lesser quantities of low-Ca pyroxene, feldspathic glass, chromite, metal, and sulfides have also been observed. There are a number of mineralogical similarities between the agglomeratic chondrules and the fine-grained SD Kool grains including olivines with high fayalite contents that poikolitically enclose Cr-rich spinels and minor Al-rich interstitial silicate glass. Kool grains, however, are typically composed of finer grain sizes than the agglomeratic chondrules and contain high Ca-pyroxenes as a principal phase. The agglomeratic chondrules were interpreted as mechanical mixtures of phases with perhaps some post-accretion sintering which produced minor quantities of interstitial glass.

Oxidation of Kool Fragment Noni-A

The mineralogy and texture of the TP from Track 58, a type A track, is composed of an inner core of Fe-oxides and Ni-oxides surrounded by submicron Ko augite, FeO-rich olivine and aluminosilicate glass as previously described. No other comparable fragments from the SD tracks have been observed indicating that this fragment is unique. Though Fe and Ni oxides clearly imply formation in a highly oxidizing environment, it is difficult to imagine a scenario where this assemblage could have formed. Ni-rich Fe oxides are observed in rocks produced by large impacts on Earth (Hart et al. 2002). Perhaps the core of Noni-A formed from melting by shock-induced impact under highly oxidizing conditions and then olivine and Ko-augite later nucleated when a silicate melt came into contact with the oxides.

Could Kool Fragments be Chondrule Precursors?

Kool fragments are composed of submicron to ~1 μm grains that formed in high temperature environments and have bulk compositions similar to type II FeO-rich chondrules in ordinary chondrites. These objects are observed in >50% of SD tracks indicating their widespread distribution in comet Wild 2. Kool fragments are also observed in chondritic porous IDPs some of which are almost certainly derived from comets. These properties of Kool fragments invoke the intriguing possibility that Kool fragments might be samples of precursor materials that accreted to form type II chondrules in ordinary chondrites. It they are precursors then why have Kool fragments not been found in OC meteorites? One explanation might be that if Kool fragments were incorporated into chondrules then it is unlikely that these fine-grained materials would survive the high temperatures of chondrule formation. Repeated recycling and subsequent grain growth would further destroy any Kool grain relicts

(Hewins and Connolly 1996; Wasson 1996). A similar explanation may account for their absence in chondrite matrix, as many UOCs even of low petrologic subtypes have experienced hydrous alteration and mild heating, which may have altered their primary grains (Huss et al. 2006). Matrix in Semarkona, for instance, a type LL3.0 chondrite, is dominated by phyllosilicates.

In addition to the lack of preservation, another possible explanation is that Kool grains did not exist at the appropriate place and time when the established chondrite types accreted. Each chondrite group has distinctive elemental, mineralogical, chemical and isotopic properties (Brearley and Jones 1998) and it is clear that these different groups formed from local materials with these distinctive properties. Besides local materials, chondrites also contain pre-solar grains, CAIs and other minor components that clearly formed elsewhere and at earlier times. Comet Wild 2 accreted at the edge of the solar system and is likely to be dominated by rocky materials that formed elsewhere and were transported beyond the orbits of all the planets. The presence of CAIs, chondrules and presolar grains in Wild 2 (Simon et al. 2008; Nakamura et al. 2008; Messenger et al. 2009) suggest that the comet formation region was a gathering place for materials produced over the full expanse of the solar nebula. Thus it is possible that chondrule precursor materials were transported to the comet accretion zone where they would have been preserved while the precursors that remained in the inner regions of the solar nebula were destroyed by chondrule formation and other processes.

Origin of the Kool Fragments

The SD Kool grains have similar bulk compositions as type II FeO-rich chondrules. Their igneous textures and fine-grained minerals which formed at temperatures typical of igneous rocks as well as the small sizes of the whole fragments suggest formation of melt droplets in a nebular environment. The apparent presence of ferric iron in some of the fragments implies formation in moderately high fO_2 conditions. We envision heating of very fine-grained materials in a chondritic region relatively rich in oxygen possibly close to the R chondrite-forming region of the nebula. Melting of dispersed fine-grained materials produced chondritic liquid droplets on a very fine scale. The droplets must not have been heated much above their liquidus temperatures preserving numerous nucleation sites for subsequent growth of fine-grained crystals. During heating an immiscible sulfide melt portion separated from the silicate liquid. In some droplets these two melts remained attached. As cooling occurred, olivine and chromite crystals began to grow. Eventually, chromite was overtaken by olivine growth and become poikilitically enclosed. With the appearance of clinopyroxene and the residual liquids being enhanced in Na and Cr, these two elements were incorporated into the clinopyroxene via coupled substitution. During the growth of clinopyroxene, chromite did not crystallize because Cr (along with Na) was incorporated into the pyroxene while only trace amounts went into olivine. Depending on the amount of Na remaining in the late-stage melt either albite crystallized (or attempted to) or Na + Al silicate glass remained. Kool fragments could have become attached to one another and formed larger grains which were utilized into chondrule formation. Some Kool grains were transported to the Kuiper belt to be preserved in comets. Those that remained were presumably destroyed during chondrule formation. Alternatively, the fine-grained SD Kool grains may not have accreted into chondrules but simply represent an unrecognized population of fine-grained early nebular materials, perhaps microchondrules that were transported to the Kuiper belt. The coarse-grained Kool fragments may have formed in regions similar to their fine-grained counterparts, perhaps where there was less shielding of heat, as they were subsequently heated allowing the growth of coarser grains and crystallization of Na-Al rich glass to albitic feldspar.

CONCLUSIONS

Terminal particles and wall fragments from 16 tracks contain a diverse assemblage of minerals, glass, CAIs, microchondrules, carbonaceous phases and pre-solar grains. Surprisingly, half contain clinopyroxenes with elevated Na and Cr contents that are significantly higher than observed in clinopyroxenes in chondrites. These kosmochloric clinopyroxenes often occur in fine-grained (submicron) assemblages composed of Ko-clinopyroxene + FeO-rich olivine ± Cr-rich spinel ± aluminosilicate glass or feldspar and have textures consistent with igneous melts. Coarse-grained (>1 μm) assemblages composed of Ko-clinopyroxene + FeO-rich olivine ± albitic feldspar were also observed. Kool grains (Ko-clinopyroxene + FeO-rich olivine ± Cr-rich spinel ± aluminosilicate glass or albitic feldspar) were also found in 4 chondritic porous IDPs which likely originated in comets. Clinopyroxenes with elevated Na and Cr contents are not found in chondrules.

The measured bulk composition of a representative fine-grained Kool fragment is similar to type II FeO-rich chondrules from ordinary chondrites. Fine-grained Kool grains may have formed from submillimeter droplets in the nebula similar to type II chondrules in OCs, but the presence of enhanced Na and Cr in the clinopyroxenes implies a different crystallization history than the chondrules. The average distribution of the major elements Fe and Mg and the minor elements Al, Ti, and Mn between co-existing Ko-clinopyroxenes and olivines within individual Kool fragments suggests that these two phases formed at near equilibrium conditions. However, the high concentrations of Na in the clinopyroxenes compared to their interstitial glasses are inconsistent with equilibrium crystallization with published distribution coefficients. Unlike chondrules from type II OCs, where Cr is largely present in chromite, a

significant portion of Cr in the Kool grains is present in clinopyroxene which may have been present in the melt phase during clinopyroxene crystallization. It is suggested that the partitioning of Na and Cr into the Kool clinopyroxenes via coupled substitution was dramatically enhanced by the availability of both cations in the melt during clinopyroxene crystallization thereby increasing the kosmochlor component in the pyroxenes. The incorporation of Cr in clinopyroxene accounts for the low modal abundance of chromite in Kool grains.

The larger grain sizes of coarse-grained Kool fragments complicate estimation of bulk composition but it is probable they have similar bulk compositions as fine-grained Kool fragments because of similar mineralogy. The coarse-grained Kool fragments are mineralogically similar to equilibrated clasts in R chondrites and may also have formed in oxidizing conditions in the nebula. An oxidized thermal metamorphic origin for coarse-grained Kool fragments is supported by the presence of FeO-rich olivine, lack of metal and possible ferric iron in the clinopyroxenes and Cr-rich spinels. Fine-grained Kool fragments are also likely to have formed in oxidizing environments.

The abundance of Kool grains in SD tracks and chondritic IDPs, their submicron to micron grain sizes, bulk compositions, as well as their overall small fragment sizes, indicates that Kool grains are good candidates as chondrule precursors to type II FeO-rich porphyritic chondrules in ordinary chondrites. Kool grains, however, have not been reported in the chondrules in OCs or for that matter in any chondrites. Their absence may suggest that Kool grains were destroyed during chondrule-processing or simply were not present in the chondrule-forming region of the nebula at the time of chondrule formation.

Acknowledgments—Thanks to Dave Lindstrom and I. S. McCallum for helpful discussions and insights and to John Bradley for organization of the Timber Cove II meeting from which many of the ideas in this paper were born or solidified. Special thanks to Adrian Brearley whose extensive and thoughtful comments greatly improved the manuscript. This work was supported by the National Aeronautics and Space Administration (NASA) grants NNG06GG00G and NNX07AM93G.

Editorial Handling—Dr. John Bradley

REFERENCES

Alexander C. M. O'D. and Grossman J. N. 2005. Alkali elemental and potassium isotopic compositions of Semarkona chondrules. *Meteoritics & Planetary Science* 40:541–556.

Barnes S. J. 1998. Chromite in komatiites, 1. Magmatic controls on crystallization and composition. *Journal of Petrology* 39:1689–1720.

Bayliss P., Berry L. G., Mrose M. E., and Smith D. D., eds. 1980. *JCPDS mineral powder diffraction file data book.* Swarthmore, PA: JCPDS International Centre for Diffraction Data.

Beckett J. R., Connolly H. C., and Ebel D. S. 2006. Chemical processes in igneous calcium-aluminum-rich inclusions: A mostly CMAS view of melting and crystallization. In *Meteorites and the early solar system II*, edited by Lauretta D. S. and McSween H. Y., Jr. Tucson: The University of Arizona Press. pp. 399–430.

Benedix G. K., McCoy T. J., Keil K., and Love S. G. 2000. A petrologic study of the IAB iron meteorites: Constraints on the formation of the IAB-winonaite parent body. *Meteoritics & Planetary Science* 35:1127–1141.

Bennett S. L., Blundy J., and Elliott T. 2004. The effect of sodium and titanium on crystal-melt partitioning of trace elements. *Geochimica et Cosmochimica Acta* 68:2335–2347.

Bischoff A., Geiger T., Palme H., Spettel B., Schultz L., Scherer B., Loeken T., Bland T., Clayton R. N., Mayeda T. K., Herpers U., Meltzow T, Michel R., and Dittrich-Hannen B. 1994. Acfer 217–A new member of the Rumuruti chondrite group (R). *Meteoritics* 29:264–274.

Blundy J. D., Falloon T. J., Wood B. J., and Dalton J. A. 1995. Sodium partitioning between clinopyroxene and silicate melts. *Journal of Geophysical Research* 100(B8):15,501–15,515.

Bradley J. P. 1994. Nanometer-scale mineralogy and petrography of fine-grained aggregates in anhydrous interplanetary dust particles. *Geochimica et Cosmochimica Acta* 58:2123–2134.

Bradley J. P. 2003. Interplanetary dust particles. In *Meteorites, comets, and planets*, edited by Davis A. Treatise on Geochemistry, vol. 1. Oxford: Elsevier-Pergamon. pp. 689–711.

Brearley A. J. and Jones R. H. 1998. Chondritic meteorites. In *Planetary materials*, edited by Papike J. J. Reviews in Mineralogy, vol. 36. Washington, D.C.: Mineralogical Society of America.

Brownlee D. E., Joswiak D. J., Love S. G., Bradley J. P., Nier A. O., and Schlutter D. J. 1994. Identification and analysis of cometary IDPs (abstract #1185). 40th Lunar and Planetary Science Conference. CD-ROM.

Brownlee D. E., Joswiak D. J., Love S. G., Nier A. O., Schlutter D. J., and Bradley J. P. 1993. Properties of cometary and asteroidal IDPs identified by He temperature-release profiles. *Meteoritics* 28:332.

Brownlee D., Tsou P., Aléon J., Alexander C. M. O'D., Araki T., Bajt S., Baratta G. A., Bastien R., Bland P., Bleuet P., Borg J., Bradley J. P., Brearley A., Brenker F., Brennan S., Bridges J. C., Browning N. D., Brucato J. R., Bullock E., Burchell M. J., Busemann H., Butterworth A., Chaussidon M., Cheuvront A., Chi M., Cintala M. J., Clark B. C., Clemett S. J., Cody G., Colangeli L., Cooper G., Cordier P., Daghlian C., Dai Z., D'Hendecourt L., Djouadi Z., Dominguez G., Duxbury T., Dworkin J. P., Ebel D. S., Economou T. E., Fakra S., Fairey S. A. J., Fallon S., Ferrini G., Ferroir T., Fleckenstein H., Floss C., Flynn G., Franchi I. A., Fries M., Gainsforth Z., Gallien J.-P., Genge M., Gilles M. K., Gillet Ph., Gilmour J., Glavin D. P., Gounelle M., Grady M. M., Graham G. A., Grant P. G., Green S. F., Grossemy F., Grossman L., Grossman J. N., Guan Y., Hagiya K., Harvey R., Heck P., Herzog G. F., Hoppe P., Hörz F., Huth J., Hutcheon I. D., Ignatyev K., Ishii H., Ito M., Jacob D., Jacobsen C., Jacobsen S., Jones S., Joswiak D., Jurewicz A., Kearsley A. T., Keller L. P., Khodja H., Kilcoyne A. L. D., Kissel J., Krot A., Langenhorst F., Lanzirotti A., Le L., Leshin L. A., Leitner J., Lemelle L., Leroux H., Liu M.-C., Luening K., Lyon I., MacPherson G., Marcus M. A., Marhas K., Marty B., Matrajt G., McKeegan K., Meibom A., Mennella V., Messenger K., Messenger S., Mikouchi T., Mostefaoui S., Nakamura T., Nakano T., Newville M., Nittler L. R., Ohnishi I.,

Ohsumi K., Okudaira K., Papanastassiou D. A., Palma R., Palumbo M. E., Pepin R. O., Perkins D., Perronnet M., Pianetta P., Rao W., Rietmeijer F. J. M., Robert F., Rost D., Rotundi A., Ryan R., Sandford S. A., Schwandt C. S., See T. H., Schlutter D., Sheffield-Parker J., Simionovici A., Simon S., Sitnitsky I., Snead C. J., Spencer M. K., Stadermann F. J., Steele A., Stephan T., Stroud R., Susini J., Sutton S. R., Suzuki Y., Taheri M., Taylor S., Teslich N., Tomeoka K., Tomioka N., Toppani A., Trigo-Rodríguez J. M., Troadec D., Tsuchiyama A., Tuzzolino A. J., Tyliszczak T., Uesugi K., Velbel M., Vellenga J., Vicenzi E., Vincze L., Warren J., Weber I., Weisberg M., Westphal A. J., Wirick S., Wooden D., Wopenka B., Wozniakiewicz P., Wright I., Yabuta H., Yano H., Young E. D., Zare R. N., Zega T., Ziegler K., Zimmermann L., Zinner E., and Zolensky M. 2006. Comet 81P/Wild 2 under a microscope. *Science* 314:1711–1716.

Buening D. K. and Buseck P. R. 1973. Fe-Mg lattice diffusion in olivine. *Journal of Geophysical Research* 78:6852–6862.

Burchell M. J., Fairey S. A. J., Wozniakiewicz P., Brownlee D. E., Hörz F., Kearsley A. T., See T. H., Tsou P., Westphal A., Green S. F., Trigo-Rodríguez J. M., and Dominguez G. 2008. Characteristics of cometary dust tracks in Stardust aerogel and laboratory calibrations. *Meteoritics & Planetary Science* 43:23–40.

Ciesla F. J. and Cuzzi J. N. 2007. Radial transport of high temperature materials in the solar nebula: applications to Stardust (abstract #1386). 38th Lunar and Planetary Science Conference. CD-ROM.

Connolly H. C. Jr. and Hewins R. H. 1996. Constraints on chondrule precursors from experimental data. In *Chondrules and the protoplanetary disk*, edited by Hewins R. H., Jones R. H., and Scott E. R. D. New York: Cambridge University Press. pp. 129–135.

Dodd R. T. 1971. The petrology of chondrules in the Sharps meteorite. *Contributions to Mineralogy and Petrology* 31:2010–227.

Dodd R. T. and Van Schmus W. R. 1971. Dark zoned chondrules. *Chemie der Erde* 30:49–69.

Duke J. M. 1976. Distribution of the period four transition elements among olivine, calcic clinopyroxene and mafic silicate liquid: experimental results. *Journal of Petrology* 17:499–521.

Ebel D. S. and Grossman L. 2000. Condensation in dust-enriched systems. *Geochimica et Cosmochimica Acta* 64:339–366.

Flynn G. J., Bleuet P., Borg J., Bradley J. P., Brenker F. E., Brennan S., Bridges J., Brownlee D. E., Bullock E. S., Burghammer M., Clark B. C., Dai Z. R., Daghlian C. P., Djouadi Z., Fakra S., Ferroir T., Floss C., Franchi I. A., Gainsforth Z., Gallien J.-P., Gillet Ph., Grant P. G., Graham G. A., Green S. F., Grossemy F., Heck P. R., Herzog G. F., Hoppe P., Hörz F., Huth J., Ignatyev K., Ishii H. A., Janssens K., Joswiak D., Kearsley A. T., Khodja H., Lanzirotti A., Leitner J., Lemelle L., Leroux H., Luening K., MacPherson G. J., Marhas K. K., Marcus M. A., Matrajt G., Nakamura T., Nakamura-Messenger K., Nakano T., Newville M., Papanastassiou D. A., Pianetta P., Rao W., Riekel C., Rietmeijer F. J. M., Rost D., Schwandt C. S., See T. H., Sheffield-Parker J., Simionovici A., Sitnitsky I., Snead C. J., Stadermann F. J., Stephan T., Stroud R. M., Susini J., Suzuki Y., Sutton S. R., Taylor S., Teslich N., Troadec D., Tsou P., Tsuchiyama A., Uesugi K., Vekemans B., Vicenzi E. P., Vincze L., Westphal A. J., Wozniakiewicz P., Zinner E., and Zolensky M. E. 2006. Elemental compositions of comet 81P/Wild 2 samples collected by Stardust. *Science* 314:1731–1735.

Freer R. 1981. Diffusion in silicate minerals and glasses: A data digest and guide to the literature. *Contributions to Mineralogy and Petrology* 76:440–454.

Geochemical Earth Reference Model, GERM Partition Coefficient (Kd) Database. http://earthref.org/cgi-bin/er.cgi?s=kdd-s0-main.cgi.

Grossman J. N. and Wasson J. T. 1983. The compositions of chondrules in unequilibrated chondrites: an evaluation of models for the formation of chondrules and their precursor materials, In *Chondrules and their origins*, edited by King E. A. Houston: Lunar and Planetary Institute. pp. 88–121.

Harlow G. E. 1996. Structure refinement of a natural K-rich diopside: The effect of K on the average structure. *American Mineralogist* 81:632–638.

Hart R. J., Cloete M., McDonald I., Carlson M., and Andreoli A. G. 2002. Siderophile-rich inclusions from the Morokweng impact melt sheet, South Africa: Possible fragments of a chondritic meteorite. *Earth and Planetary Science Letters* 198:49–62.

Henderson P. 1982. *Inorganic geochemistry.* Oxford: Pergamon Press. 353 p.

Hewins R. H. and Connolly H. C. Jr. 1996. Peak temperatures of flash-melted chondrules. In *Chondrules and the protoplanetary disk*, edited by Hewins R. H., Jones R. H., and Scott E. R. D. New York: Cambridge University Press. 197–204.

Hörz F., Zolensky M. E., Bernhard R. P., See T. H., and Warren J. L. 2000. Impact features and projectile residues in aerogel exposed on MIR. *Icarus* 147:559–579.

Huang F., Lundstrom C. C., and McDonough W. F. 2006. Effect of melt structure on trace-element partitioning between clinopyroxene and silicic alkaline, aluminous melts. *American Mineralogist* 91:1385–1400.

Huss G. R., Rubin A. E., and Grossman J. N. 2006. Thermal metamorphism in chondrites. In *Meteorites and the early solar system II*, edited by Lauretta D. S. and McSween H. Y. Jr. Tucson: The University of Arizona Press. pp. 567–586.

Jones R. H. 1990. Petrology and mineralogy of Type II, FeO-rich chondrules in Semarkona (LL 3.0): Origin by closed-system fractional crystallization, with evidence for supercooling. *Geochimica et Cosmochimica Acta* 54:1785–1802.

Jones R. H. 1996. FeO-rich porphyritic pyroxene chondrules in unequilibrated ordinary chondrites. *Geochimica et Cosmochimica Acta* 60:3115–3138.

Jones R. H. and Layne G. D. 1997. Minor and trace element partitioning between pyroxene and melt in rapidly cooled chondrules. *American Mineralogist* 82:534–545.

Joswiak D. J., Brownlee D. E., Pepin R. O., and Schlutter D. J. 2005. Densities and mineralogy of cometary and asteroidal interplanetary dust particles collected in the stratosphere. Proceedings, Workshop on Dust in Planetary Systems, Kauai, Hawaii, USA. pp. 141–144.

Joswiak D. J., Brownlee D. E., and Matrajt G. 2007. Mineralogy of terminal particles and other large mineral fragments obtained from Stardust tracks (abstract #5256). *Meteoritics & Planetary Science* 42:A78.

Joswiak D. J., Matrajt G., Brownlee D. E., Westphal A. J., and Snead C. J. 2007. A roedderite-bearing terminal particle from Stardust Track 56: Comparison with rare peralkaline chondrules in ordinary chondrites. 38th Lunar and Planetary Science Conference (abstract # 1338). CD-ROM.

Kallemeyn G. W., Rubin A. E., and Wasson J. T. 1996. The compositional classification of chondrites: VII. The R chondrite group. *Geochimica et Cosmochimica Acta* 60:2243–2256.

Karner J. M., Papike J. J., Sutton S. R., Shearer C. K., McKay G., Le L. and Burger P. 2007. Valence state partitioning of Cr between pyroxene-melt: Effects of pyroxene and melt composition and direct determination of Cr valence states by XANES. Application to Martian basalt QUE 94201 composition. *American Mineralogist* 92:2002–2005.

Keller L. P. and Messenger S. M. 2009. Equilibrated aggregates in cometary IDPs: Insights into the crystallization process in protoplanetary disks. 40th Lunar and Planetary Science Conference (abstract # 2121). CD-ROM.

Kimura M. and Yagi K. 1980. Crystallization of chondrules in ordinary chondrites. *Geochimica et Cosmochimica Acta* 44:589–602.

Klöck W. and Stadermann F. J. 1994. Mineralogical and chemical relationships of interplanetary dust particles, micrometeorites and meteorites. *Analysis of interplanetary dust*, edited by Zolensky E., Wilson T. L., Rietmeijer F. J. M., and Flynn G. J. P. AIP Conference Proceedings, vol. 310. New York: American Institute of Physics. pp. 51–87.

Krot A. N., Rubin A. E., Keil K., and Wasson J. T. 1997. Microchondrules in ordinary chondrites: Implications for chondrule formation. *Geochimica et Cosmochimica Acta* 61:463–473.

Krot A. N. and Wasson J. T. 1994. Silica-merrihueite/roedderite-bearing chondrules and clasts in ordinary chondrites: New occurrences and possible origin. *Meteoritics* 29:707–718.

Lauretta D. S., Nagahara H., and Alexander C. M. O'D 2006. Petrology and origin of ferromagnesian silicate chondrules. In *Meteorites and the early solar system II*, edited by Lauretta D. S. and McSween H. Y. Jr. Tucson: The University of Arizona Press. pp. 432–459.

Lanzirotti A., Sutton S. R., Flynn G. J., Newville M., and Rao W. 2008. Chemical composition and heterogeneity of Wild 2 cometary particles determined by synchrotron X-ray fluorescence. *Meteoritics & Planetary Science* 43:187–213.

Leroux H., Rietmeijer F. J. M., Velbel M. A., Brearley A. J., Jacob D., Langenhorst F., Bridges J. C., Zega T. J., Stroud R. M., Cordier P., Harvey R. P., Lee M., Gounelle M., and Zolensky M. E. 2008. A TEM study of thermally modified comet 81P/Wild 2 dust particles by interactions with the aerogel matrix during the Stardust capture process. *Meteoritics & Planetary Science* 43:97–120.

Lofgren G. E. 1996. A dynamic crystallization model for chondrule melts. In *Chondrules and the protoplanetary disk*, edited by Hewins R. H., Jones R. H., and Scott E. R. D. New York: Cambridge University Press. pp. 187–196.

Love S. G. and Brownlee D. E. 1994. Peak atmospheric entry temperature of micrometeorites. *Meteoritics* 29:69–70.

Lundstrom C. C., Shaw H. F., Ryerson F. J., Williams Q., and Gill J. 1998. Crystal chemical control of clinopyroxene-melt partitioning in the Di-Ab-An system: Implications for elemental fractionations in the depleted mantle. *Geochimica et Cosmochimica Acta* 62:2849–2862.

Mahood G. A. and Stimac J. A. 1990. Trace-element partitioning in pantellerites and trachytes. *Geochimica et Cosmochimica Acta* 54:2257–2276.

Maity S., Bhattacharya P., and Gupta A. K. 1997. Preliminary phase equilibria study on the join forsterite-diopside-albite under 10 and 20 Kb at variable temperatures and its significance. In *The dynamic geosphere*, edited by Gupta A. K. and Kerrich R. Mumbai: Allied Publishers. pp. 44–55.

Matrajt G. and Brownlee D. E. 2006. Acrylic embedding of Stardust particles encased in aerogel. *Meteoritics & Planetary Science* 41: 1715–1720.

Matrajt G., Ito M., Wirick S., Messenger S., Brownlee D. E., Joswiak D., Flynn G., Sandford S., Snead C., and Westphal A. 2008. Carbon investigation of two Stardust particles: A TEM, NanoSIMS and XANES study. *Meteoritics & Planetary Science* 43:315–334.

McCoy T. J., Ehlmann A. J., Benedix G. K., Keil K., and Wasson J. T. 1996. The Lueders, Texas, IAB iron meteorite with silicate inclusions. *Meteoritics & Planetary Science* 31:419–422.

Messenger S., Joswiak D., Ito M., Matrajt G., and Brownlee D. E. 2009. Discovery of presolar SiC from comet Wild 2 (abstract #1790). 40th Lunar and Planetary Science Conference. CD-ROM.

Morimoto N., Fabries J., Ferguson A. K., Gizburg I. V., Ross M., Seifert F. A., Zussman J., Aoki K., and Gottardi G. 1988. Nomenclature of pyroxenes. *American Mineralogist* 73:1123–1133.

Morse S. A. 1980. *Basalts and phase diagrams. An introduction to the quantitative use of phase diagrams in igneous petrology*, Berlin: Springer-Verlag. 493 p.

Mysen B. O. and Virgo D. 1980. Trace element partitioning and melt structure: an experimental study at 1 atm pressure. *Geochimica et Cosmochimica Acta* 44:1917–1930.

Nakamura T, Noguchi T., Tsuchiyama A., Ushikubo T., Kita N. T., Valley J. W., Zolensky M. E., Kakazu Y., Sakamoto K., Mashio E., Uesugi K., and Nakano T. 2008. Chondrule-like objects in short-period comet 81P/Wild 2. *Science* 321:1664–1667.

Noguchi T., Nakamura T., Okudaira, K., Yano, H., Sugita S., and Burchell M. J. 2007. Thermal alteration of hydrated minerals during hypervelocity capture to silica aerogel at the flyby speed of Stardust. *Meteoritics & Planetary Science* 42:357–372.

Okuno M. and Marumo F. 1982. The structures of anorthite and albite melts. *Mineralogical Journal* 11:180–196.

Olson E. J. and Schwade J. 1998. The silicate inclusions of the Ocotillo IAB iron meteorite. *Meteoritics & Planetary Science* 33: 153–155.

Peltonen P. 1995. Crystallization and re-equilibration of zoned chromite in ultramafic cumulates, Vammala Ni-belt, southwestern Finland. *The Canadian Mineralogist* 33:521–535.

Rietmeijer F. J. M. 1998. Interplanetary dust particles. In *Planetary materials*, edited by Papike J. J. Reviews in Mineralogy, vol. 36. Washington, D.C.: Mineralogical Society of America.

Roskosz M., Leroux H., and Watson H. C. 2008. Thermal history, partial preservation and sampling bias recorded by Stardust cometary grains during their capture. *Earth and Planetary Science Letters* 273:195–202.

Rubin A. E. 1984. Coarse-grained chondrule rims in type 3 chondrites. *Geochimica et Cosmochimica Acta* 48:1779–1789.

Rubin A. E. and Kallemeyn G. W. 1994. Pecora Escarpment 91002: A member of the new Rumuruti (R) chondrite group. *Meteoritics* 29:255–264.

Ruzicka A., Fowler G. W., Snyder G. A., Prinz M., Papike J. J., and Taylor L. A. 1999. Petrogenesis of silicate inclusions in the Weekeroo Station IIE iron meteorite: Differentiation, remelting, and dynamic mixing. *Geochimica et Cosmochimica Acta* 63: 2123–2143.

Schairer J. J. and Morimoto N. 1958. Systems with rock forming olivines, pyroxenes and feldspars. *Carnegie Institute of Washington Yearbook* 57:212–213.

Schulze H., Bischoff A., Palme H., Spettel B., Dreibus G., and Otto J. 1994. Mineralogy and chemistry of Rumuruti: The first meteorite fall of the new R chondrite group. *Meteoritics* 29:275–286.

Scott E. R. D. and Krot A. N. 2003. Chondrites and their components. In *Meteorites, comets, and planets*, edited by Davis A. Treatise on Geochemistry, vol. 1. Oxford: Elsevier-Pergamon. pp. 143–200.

Scott E. R.D. and Krot A. N. 2005. Chondritic meteorites and the high-temperature nebular origins of their components. In *Chondrites and the protoplanetary disk*, edited by Krot A. K., Scott E. R. D., and Reipurth B. ASP Conference Series, vol. 341. Provo, Utah: Brigham Young University. pp. 15–53.

Shu F. H., Shang H., Glassgold A. E., and Lee T. 1997. X-rays and fluctuating X-winds from protostars. *Science* 277:1475–1479.

Simon S. B., Joswiak D., Ishii H. A., Bradley J. P., Chi M., Grossman L., Aléon J., Brownlee D. E., Fallon S., Hutcheon I. D., Matrajt

G., and McKeegan K. D. 2008. A refractory inclusion returned by Stardust from comet 81P/Wild 2. *Meteoritics & Planetary Science* 43:1861–1877.

Stephan T., Flynn G. J., Sandford S. A., and Zolensky M. E. 2008. TOF-SIMS analysis of cometary particles extracted from Stardust aerogel. *Meteoritics & Planetary Science* 43:285–298.

Takeda H., Hsu W., and Huss G. R. 2003. Mineralogy of silicate inclusions of the Colomera IIE iron and crystallization of Cr-diopside and alkali feldspar from a partial melt. *Geochimica et Cosmochimica Acta* 67:2269–2288.

Takeda H., Mori H., and Ogata H. 1989. Mineralogy of augite-bearing ureilites and the origin of their chemical trends. *Meteoritics* 24:73–81.

Tsujimore T. and Liou J. G. 2005. Low-pressure and low-temperature K-bearing kosmochloric diopside from the Osayama serpentinite mélange, SW Japan. *American Mineralogist* 90:1629–1635.

Uhlmann D. R., Yinnon H., and Dranmer D. 1980. Crystallization behavior of albite (abstract). 11th Lunar and Planetary Science Conference. pp. 1178–1180.

Van Schmus W. R. 1969. The mineralogy and petrology of chondritic meteorites. *Earth Science Reviews* 5:145–184.

Wasson J. T. 1996. Chondrule formation: Energetics and length scales. In *Chondrules and the protoplanetary disk*, edited by Hewins R. H., Jones R. H., and Scott E. R. D. New York: Cambridge University Press. pp. 45–54.

Wasson J. T. and Rubin A. E. 2003. Ubiquitous low-FeO relict grains in type II chondrules and limited overgrowths on phenocrysts following the final melting events. *Geochimica et Cosmochimica Acta* 67:2239–2250.

Weisberg M. K. and Prinz M. 1996. Agglomeratic chondrules, chondrule precursors, and incomplete melting. In *Chondrules and the protoplanetary disk*, edited by Hewins R. H., Jones R. H., and Scott E. R. D. New York: Cambridge University Press. pp. 119–127.

Weisberg M. K., Prinz M., Kojima H., Yanai K., Clayton R. N., and Mayeda T. K. 1991. The Carlisle Lakes-type chondrites: A new grouplet with high ^{17}O and evidence for nebular oxidation, *Geochimica et Cosmochimica Acta* 55:2657–2669.

Westphal A. J., Snead C. J., Butterworth A. L., Graham G. A., Bradley J. P., Bajt S., Grant P. G., Bench G., Brennan S., and Pianetta P. 2004. Aerogel keystones: Extraction of complete hypervelocity impact events from aerogel collectors. *Meteoritics & Planetary Science* 39:1375–1386.

Wood J. A. and Holmberg B. B. 1994. Constraints placed on the chondrule-forming process by merrihueite in the Mezö-Madaras chondrite. *Icarus* 108:309–324.

Zolensky M. E., Zega T. J., Yano H., Wirick S., Westphal A. J., Weisberg M. K., Weber I., Warren J. L., Velbel M. A., Tsuchiyama A., Tsou P., Toppani A., Tomioka N., Tomeoka K., Teslich N., Taheri M., Susini J., Stroud R., Stephan T., Stadermann F. J., Snead C. J., Simon S. B., Simionovici A., See T. H., Robert F., Rietmeijer F. J. M., Rao W., Perronnet M. C., Papanastassiou D. A., Okudaira K., Ohsumi K., Ohnishi I., Nakamura-Messenger K., Nakamura T., Mostefaoui S., Mikouchi T., Meibom A., Matrajt G., Marcus M. A., Leroux H., Lemelle L., Le L., Lanzirotti A., Langenhorst F., Krot A. N., Keller L. P., Kearsley A. T., Joswiak D., Jacob D., Ishii H., Harvey R., Hagiya K., Grossman L., Grossman J. N., Graham G. A., Gounelle M., Gillet Ph., Genge M. J., Flynn G., Ferroir T., Fallon S., Ebel D. S., Dai Z. R., Cordier P., Clark B., Chi M., Butterworth A. L., Brownlee D. E., Bridges J. C., Brennan S., Brearley A., Bradley J. P., Bleuet P., Bland P. A., and Bastien R. 2006. Mineralogy and petrology of comet 81P/Wild 2 nucleus samples. *Science* 314:1735–1739.